Modification of Cyclic Nucleotide–gated Ion Channels by Ultraviolet Light

Thomas R. Middendorf,*‡ Richard W. Aldrich,‡ and Denis A. Baylor*

From the *Neurobiology Department, and ‡Department of Molecular and Cellular Physiology, and Howard Hughes Medical Institute, School of Medicine, Stanford University, Stanford, California 94305

abstract We irradiated cyclic nucleotide–gated ion channels in situ with ultraviolet light to probe the role of aromatic residues in ion channel function. UV light reduced the current through excised membrane patches from *Xenopus* oocytes expressing the α subunit of bovine retinal cyclic nucleotide–gated channels irreversibly, a result consistent with permanent covalent modification of channel amino acids by UV light. The magnitude of the current reduction depended only on the total photon dose delivered to the patches, and not on the intensity of the exciting light, indicating that the functionally important photochemical modification(s) occurred from an excited state reached by a one-photon absorption process. The wavelength dependence of the channels' UV light sensitivity (the action spectrum) was quantitatively consistent with the absorption spectrum of tryptophan, with a small component at long wavelengths, possibly due to cystine absorption. This spectral analysis suggests that UV light reduced the currents at most wavelengths studied by modifying one or more "target" tryptophans in the channels. Comparison of the channels' action spectrum to the absorption spectrum of tryptophan in various solvents suggests that the UV light targets are in a water-like chemical environment. Experiments on mutant channels indicated that the UV light sensitivity of wild-type channels was not conferred exclusively by any one of the 10 tryptophan residues in a subunit. The similarity in the dose dependences of channel current reduction and tryptophan photolysis in solution suggests that photochemical modification of a small number of tryptophan targets in the channels is sufficient to decrease the currents.

key words: cyclic guanine monophosphate • electrophysiology • ligand-gated • ion channel gating • ultraviolet light

INTRODUCTION

Electrical signals in visual and olfactory transduction arise from changes in the activity of cyclic nucleotide–gated (CNG)[1] ion channels (Yau and Baylor, 1989). Opened directly by the binding of cyclic nucleotides, these channels transduce changes in the intracellular concentration of nucleotide ligands into changes in membrane potential. The channels are well suited for their roles in transduction: their cooperative activation by the binding of multiple ligand molecules makes them sensitive detectors of small changes in cyclic nucleotide concentration.

Measurements of the cyclic nucleotide dependence of currents in photoreceptors (Fesenko et al., 1985; Haynes et al., 1986; Zimmerman and Baylor, 1986) and olfactory cilia (Nakamura and Gold, 1987) provided initial insights into the molecular basis of CNG channel activation. More recent results revealed significant differences in the activation characteristics of retinal and olfactory CNG channels cloned from various species (Kaupp et al., 1989; Dhallan et al., 1990; Ludwig et al., 1990; Goulding et al., 1992). Studies of the activation of mutant and chimeric channels constructed from these original clones have identified regions of the protein sequence that comprise parts of the channels' gating machinery. These regions include the consensus cGMP binding domain near the channel's COOH terminus (Altenhofen et al., 1991; Goulding et al., 1994; Varnum et al., 1995; Gordon et al., 1996), the N-S2 domain near the channel's NH_2 terminus (Goulding et al., 1994; Liu et al., 1994; Gordon and Zagotta, 1995b; Tibbs et al., 1997), the C-linker (an ~90 amino acid sequence between the sixth transmembrane segment and the cyclic nucleotide binding domain) (Finn et al., 1995; Gordon and Zagotta, 1995a,b; Kramer and Tibbs, 1996; Zong et al., 1998; Paoletti et al., 1999), and residues in the channel pore (Bucossi et al., 1997; Fodor et al., 1997a,b).

Do other regions of CNG channels participate in channel gating? What are their energetic contributions to channel activation? It may be difficult to answer these questions using conventional mutagenesis techniques because of an inherent limitation of such approaches: functional assays may yield no detectable signal if the mutation disrupts a residue that is critical to the correct targeting, folding, or activity of the protein. These problems have been partially overcome by the use of chemical reagents to modify the reactive groups (generally the thiol function of cysteine residues) of expressed channels (Akabas et al., 1992; Finn et al., 1995;

Address correspondence to Richard W. Aldrich, Department of Molecular and Cellular Physiology, Howard Hughes Medical Institute, Stanford University, Stanford, CA 94305. Fax: 650-725-4463; E-mail: raldrich@leland.stanford.edu

[1]*Abbreviations used in this paper:* CNG, cyclic nucleotide–gated; RET channel, bovine retinal CNG channel; FWHM, full-width at half-maximum; I-D, current–dose; NATrpA, *N*-acetyl l-tryptophanamide.

Sun et al., 1996; Gordon et al., 1997; Brown et al., 1998; Lynch, 1998; Becchetti et al., 1999) or suppressor tRNA techniques (Saks et al., 1996) that allow more subtle alterations of channel amino acids (Noren et al., 1989; Nowak et al., 1998). We describe here an alternate approach that uses UV light as a chemical reagent to modify channel residues covalently in situ.

Photochemical reactivity is a property of many organic compounds (Calvert and Pitts, 1966; Turro, 1978), familiar examples being the cross linking of DNA by UV light (Setlow, 1961; McLaren and Shugar, 1964) and the photobleaching of dye molecules by visible light (Peters et al., 1974). Before the development of modern mutagenesis methods, UV modification was a primary method used to alter the sidechains of amino acids in proteins (McLaren and Shugar, 1964; Vladimirov et al., 1970; Grossweiner, 1976). The presumed mechanism of photochemical modification is depicted in Fig. 1, using the aromatic amino acid tryptophan as an example. Absorption of a UV photon promotes tryptophan from its ground electronic state to a metastable excited electronic state. The excited species is reactive, and may deactivate by transformation into a stable, covalently modified product. The identity of these products and their probability of formation depend upon many factors, including the wavelength of the UV light (Setlow and Doyle, 1957), the nature of the excited electronic state (Creed, 1984a), the identity and location of other reactive groups in the vicinity of the chromophore (Tallmadge and Borkman, 1990), the temperature (Setlow and Doyle, 1954), and the pH and concentration of dissolved oxygen in the preparation (McLaren and Pearson, 1949; Hibbard et al., 1985). UV irradiation of tryptophan in aerated aqueous solution at neutral pH generates five major stable products: kynurenine, serine, tryptamine, aspartic acid, and *N*-formyl kynurenine (Creed, 1984a). Electrons ejected from photoexcited tryptophans may also react with nearby residues in proteins (Vladimirov et al., 1970). At the wavelengths used in our study (250 nm $\leq \lambda \leq$ 330 nm), UV light also modifies cysteine and cystine residues (Augenstine and Ghiron, 1961; McLaren and Luse, 1961; Creed, 1984c) as well as the aromatic amino acids tyrosine (Kazutomo, 1955; Creed, 1984b) and phenylalanine (Cooper and Davidson, 1965; Fujimori, 1966).

We used UV modification to assess the role of aromatic residues in CNG channel function. UV dramatically reduced the cyclic nucleotide–dependent current through *Xenopus* oocyte membrane patches containing functional bovine retinal (RET) CNG channels. The dose dependence of the current reduction varied with the intensity and wavelength of the exciting light in a manner consistent with the absorption of single photons by tryptophan residues in an aqueous environment. The following paper (Middendorf and Aldrich, 2000) shows that UV reduces ionic currents through the channels by altering their gating energetics without altering their unitary conductance significantly.

MATERIALS AND METHODS

Heterologous Channel Expression

The bovine rod photoreceptor channel cDNA was cloned from a bovine retinal cDNA library by PCR amplification using oligonucleotide primers that were designed based on the published sequence (Kaupp et al., 1989). The coding sequence differs from that of Kaupp et al., (1989) by an Ala 483 to Val substitution. Messenger RNA was prepared by in vitro transcription of HindIII-linearized cDNA using the mMessage Machine kit (Ambion Corp.). The mRNA was routinely checked for degradation by agarose gel electrophoresis.

Channel proteins were expressed in *Xenopus* oocytes by microinjection of 40–80 nl of mRNA at a concentration of 0.1–1 mg/ml. Injected oocytes were incubated at 18°C in ND96 pseudoextracellular solution. This solution contained (mM) 96 NaCl, 2 KCl, 1.8 $CaCl_2$, 1 $MgCl_2$, 5 HEPES, 2.5 Na pyruvate, and 1% penicillin/streptomycin. For some experiments, oocytes were incubated at room temperature after injection to increase the rate of channel expression.

Electrical Recordings/Solutions

Macroscopic currents through excised, inside-out membrane patches from *Xenopus* oocytes expressing RET CNG channels were recorded 2–21 d after injection. The initial resistances of the borosilicate patch pipets were 0.6–5 MΩ. To minimize attenuation of the UV light reaching the patches, the tips of the pipets were not coated with sylgard or other dielectrics. Membrane currents were recorded by an Axopatch 200 patch clamp amplifier (Axon Instruments, Inc.), filtered at 2 kHz, and acquired at 10 kHz by an analog-to-digital converter (Instrutech) interfaced with a Macintosh computer (Apple Computer), using Pulse software (HEKA Corp.).

Electrical recordings were made in a perfusion chamber whose top and bottom surfaces were of optical quality quartz for high UV light transmission. Unless otherwise indicated, macroscopic ionic currents were measured in symmetrical sodium solutions. The standard sodium solution contained (mM) 130 NaCl, 3 HEPES, 0.1 EDTA, pH 7.6 (NaOH). Cyclic GMP (Sigma-Aldrich) was present in the bath (intracellular) solution at concentrations ranging from 0 to 20 mM. Solution changes were made by a gravity-driven perfusion system, and required ~30 s. The patches were held at 0 mV and outward currents were recorded at +50 mV. Current amplitudes were taken as the average value of the current during the 76-ms depolarizing pulse, omitting points within 0.5 ms of the step onset. In some experiments, there was a time-dependent droop in the currents upon depolarization, presumably due to ion accumulation/depletion effects (Zimmerman et al., 1988). For those trials, the current amplitude was estimated from the average current between 0.5 and 1.5 ms after the depolarizing voltage step. Cyclic GMP–activated currents were obtained as the difference between currents in the presence and absence of cGMP. Experiments were carried out under fluorescent room lights at 22–25°C.

Relative monovalent cation permeabilities were estimated from currents recorded under biionic conditions. The pipet contained the standard sodium solution described above, while the bath solution substituted 130 mM of NH_4Cl, KCl, LiCl, RbCl, or CsCl for NaCl, and also contained 500 μM cGMP (a nearly saturating concentration). Leak currents were recorded in otherwise identical solutions lacking cGMP.

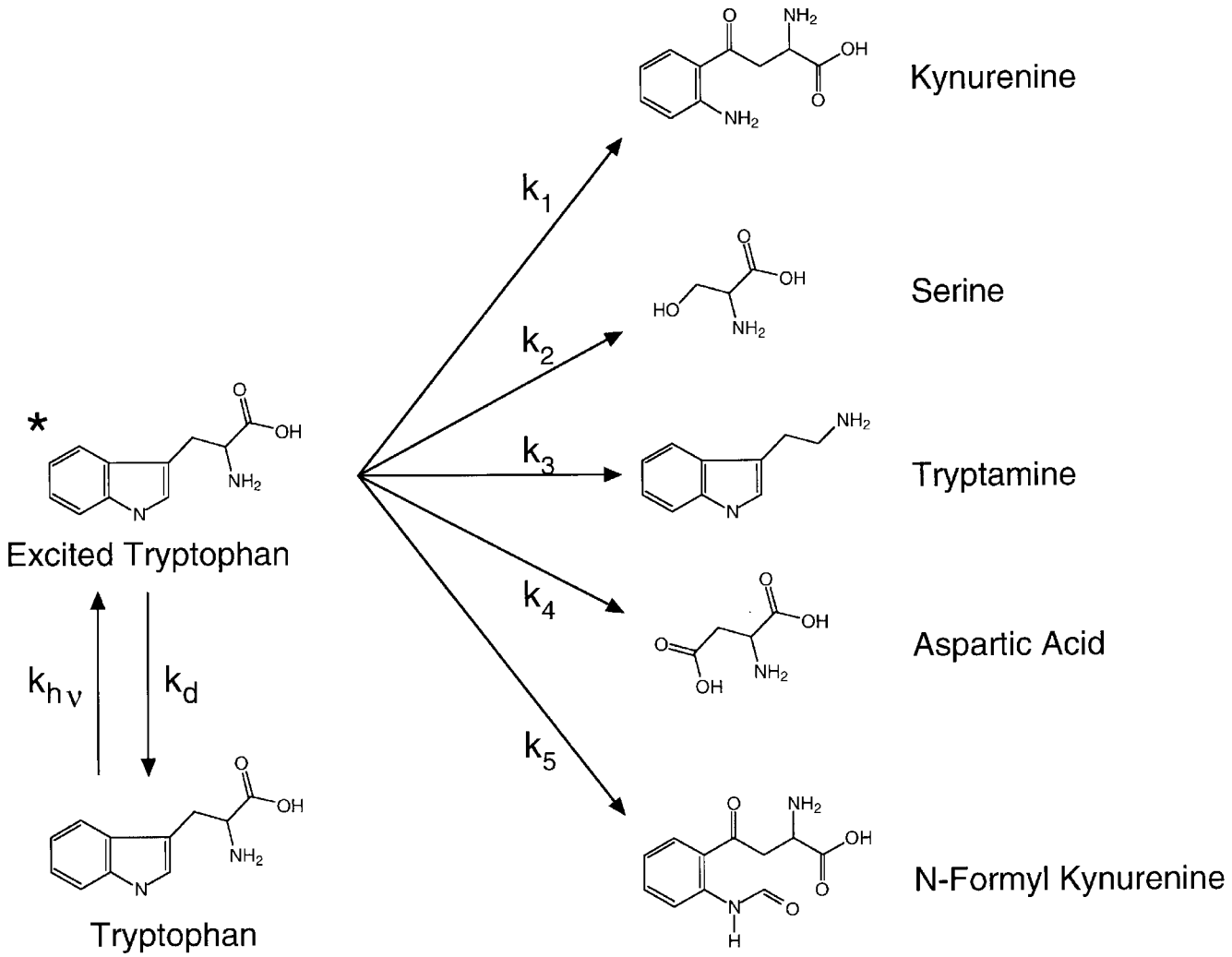

Figure 1. Schematic for photochemical modification of tryptophan. At room temperature, tryptophan molecules occupy the electronic ground state almost exclusively (bottom left). Absorption of a UV photon promotes tryptophan to an excited electronic state (*). The lifetime of the excited state is several nanoseconds (Beechem and Brand, 1985). The excited tryptophan may decay back to the ground state by a number of paths; the sum of the rate constants for these deactivation pathways is denoted k_d. Alternatively, the reactive excited molecule may form a covalently modified product by deactivating along one of the photochemical reaction pathways indicated by the rate constants k_1 through k_5. The major products of the UV photolysis of free tryptophan in aqueous solution include kynurenine, serine, tryptamine, aspartic acid, and *N*-formyl kynurenine (Creed, 1984a). The photochemical reactivity depicted here is a general property of organic molecules. We exploited this reactivity by using UV light to "mutagenize" functional ion channel proteins in situ while observing simultaneously the effect on macroscopic ionic currents through the channels.

UV Irradiation

Two different UV light sources were used. High-intensity UV was obtained from a pulsed laser. The fundamental infrared emission (1,064 nm) of a Q-switched Nd^{+3}:YAG laser (DCR-I; Quanta Ray) was frequency doubled in a second harmonic generator (SHG) crystal. The 532-nm output of this crystal was frequency doubled in a second SHG crystal, yielding 266-nm pulses of 3-ns duration with typical peak intensities of 1.7×10^{16} photons $\cdot\ \mu m^{-2} \cdot s^{-1}$ (= 12.7 mW $\cdot\ \mu m^{-2}$). Residual light at 1,064 and 532 nm was eliminated by dichroic mirrors. The laser linewidth was ~0.01 nm full width at half-maximum (FWHM).

Low-intensity UV light was obtained from a continuous-wave xenon arc lamp system (Oriel Corp.) using a stabilized power supply (#68806; Oriel Corp.). The broad-band output from the lamp was collected and collimated with an F/1 fused silica lens. The spectral composition of the UV light reaching the preparation was controlled using a combination of calibrated interference and long-pass filters (Oriel Corp. and Omega Optical). The spectral width of the excitation light was typically 10 nm FWHM. A bulb with a coated envelope that attenuated the UV output below 230 nm was used to minimize the formation of reactive ozone in the perfusion solution. No attempt was made to control the polarization of the light.

The collimated excitation light from either source was directed onto the preparation by reflection off an aluminum first-surface mirror (Newport Corp.) mounted in place of the condenser of an inverted microscope (Axiovert 35M; Carl Zeiss, Inc.). Excitation light from the arc lamp was refocused onto the preparation with a 2.5-cm focal length quartz lens, giving a typi-

cal unattenuated light intensity at the patch of 3×10^8 photons · $\mu m^{-2} \cdot s^{-1}$ ($= 0.21$ nW · μm^{-2}) at 280 nm. The final focusing lens was omitted when the pulsed laser was used. Exposure times were controlled to the nearest millisecond by an electromechanical shutter (Uniblitz Model; Vincent Associates).

The UV power densities for the arc lamp were estimated by mounting a calibrated 50-μm diameter stainless-steel pinhole (Melles Griot) in the experimental chamber at the position of the tip of the patch pipet. The power of the beam passing through the pinhole was measured with a calibrated radiometer (#222; Graseby Optronics). The spatial homogeneity of the beam was estimated by mounting a 10-μm diameter pinhole in the light path; the transmitted power at various locations within a 250×250-μm area centered on the preparation was constant to within 11%. At a fixed location, the beam power drifted by <3% over 30 min. The laser power density was determined by directing the collimated beam through a hole of defined area in an opaque block outside the sample chamber and measuring the power of the transmitted beam with a calibrated calorimetric power meter (MC 2500; Scientech, Inc.).

Attenuation of UV light by absorption in the glass walls of the patch pipets was <6%, as calculated by scaling the UV transmittance of thin glass coverslips to the pathlength of the pipet walls (<2 μm). Consistent with the very small calculated attenuation, there was no correlation between a patch's apparent UV sensitivity and the pipet wall thickness. Power densities at the patches were also corrected for reflective losses (~4.5%) at the air-quartz and quartz-water interfaces in the chamber.

Absorption Spectra

Absorption spectra of the near-UV absorbing amino acids were obtained using compounds of the highest commercially available purity: l-tryptophan (99% Sigma-Aldrich); l-tyrosine, l-phenylalanine, l-histidine, l-cysteine hydrochloride monohydrate, and l-cystine (>99%; Sigma-Aldrich); *N*-acetyl l-tryptophanamide and *N*-acetyl l-tyrosineamide (Bachem Bioscience); Ala-Tyr, and Tyr-Ala (Sigma-Aldrich).

Absorption spectra were recorded at room temperature in a single-beam UV/visible spectrophotometer (#DU 640; Beckman Instruments) and were obtained as the difference between the spectrum of the chromophore in the indicated solvent and that of the solvent alone. Samples were contained in a 1-cm pathlength fused quartz cuvette (Spectrocell) or a specially made 11-cm pathlength cell. Possible distortions in the spectra were avoided by scanning the wavelength at progressively slower speeds until there were no discernible changes in lineshape or peak position. Spectra were recorded within 1 h of sample preparation to minimize oxidation or other degradation of the sample. Extinction coefficients were obtained by dividing the absorbance by the product of the sample pathlength and concentration, and were similar to published values where available. In some cases, spectra were averaged up to 10× to enhance the signal-to-noise ratio at wavelengths with very low absorbances.

Accurate determination of absorption spectra over the full range of wavelengths tested (250–330 nm) was complicated on the long wavelength side of the spectra by a pronounced tail that was presumably caused by light scattering. The onset of the tail corresponds to the abrupt change in the curvature of the tryptophan absorption spectrum at $\lambda > 320$ nm (Fig. 2 A).

A clue to the physical origin of the tail came from the observation that it occurred at different wavelengths for the various compounds studied, but always appeared at wavelengths of low sample absorption. In a spectrophotometer, light scattering by a solute decreases the transmitted light intensity in a manner that is indistinguishable from true light absorption. Because of the exponential relation between transmitted light intensity and absorbance, the relative absorbance error introduced by this artifact is greatest when the true sample absorbance is very low. It is likely in Fig. 2 A that the true tryptophan absorbance beyond 320 nm is masked by a much larger apparent absorbance due to light scattering.

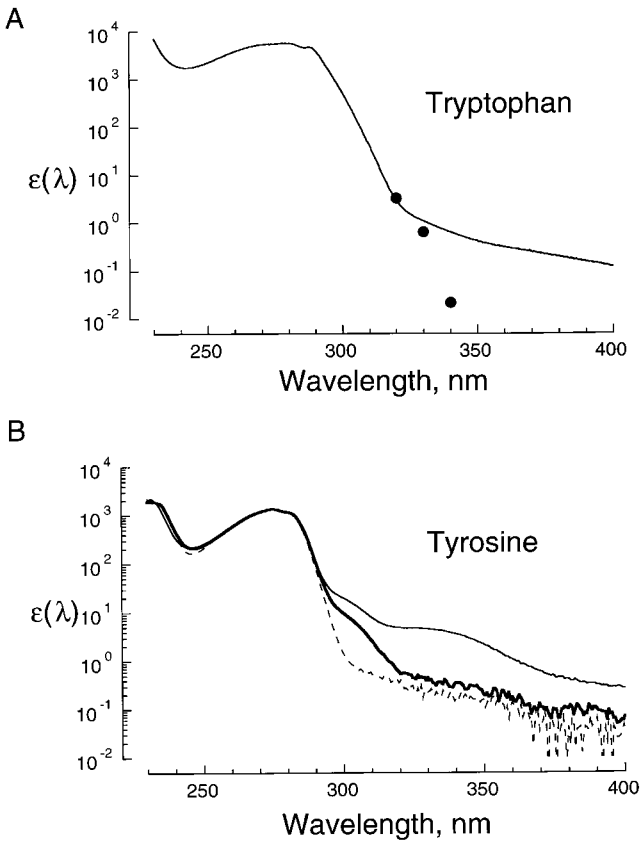

Figure 2. Removal of scattering and contaminant artifacts from tryptophan and tyrosine absorption spectra. (A) Absorption spectrum of tryptophan in standard sodium solution at pH 7.6. The solid trace is the spectrum of 312 μM tryptophan from 225 to 310 nm spliced onto that of 27 mM tryptophan from 310 to 400 nm. The extinction coefficient ($M^{-1} \cdot cm^{-1}$) was computed from the absorbance using Beer's law (Eq. 44), and is plotted as a function of wavelength in nanometers on semi-logarithmic coordinates. Also shown is the fluorescence excitation spectrum of 42 mM tryptophan from 320 to 340 nm (●) scaled to match the absorption spectrum at 320 nm. The emission wavelength for the fluorescence excitation spectrum was 360 nm. (B) Absorption spectra of tyrosine and related compounds in aqueous solution. The extinction coefficients of tyrosine (143 μM, thin line) and the dipeptide Tyr-Ala (129 μM, bold line) in standard sodium solution, pH 7.6, are plotted as a function of wavelength on semi-logarithmic axes. Also shown is the spectrum of Tyr-Ala (129 μM, dashed line) in the same solvent at pH 5.6. The Tyr-Ala spectra were scaled to the same amplitude as the tyrosine spectrum at 275.6 nm to facilitate comparison.

The hypothesis that the tail arose from scattering was further tested by measuring tryptophan's fluorescence excitation spectrum, which is not subject to light scattering artifacts. For a molecule possessing a single emitting level whose fluorescence quantum yield is independent of the exciting wavelength, the fluorescence intensity at a fixed detection wavelength is expected to vary in direct proportion to the absorption cross-section at the

excitation wavelength. The intensity of tryptophan fluorescence in a 10-nm interval centered at the peak emission wavelength (360 nm) was measured in a specially made fluorimeter. Tryptophan's fluorescence excitation spectrum, scaled to match its absorption spectrum at 320 nm, is shown by the solid circles in Fig. 2 A. The absorption estimated from the fluorescence excitation spectrum was smaller than the measured absorbance by a factor of two at 330 nm and by a factor of 30 at 340 nm. These results confirm the idea that light scattering caused the tail in the absorption spectrum at $\lambda > 320$ nm. A corrected tryptophan absorption spectrum (Fig. 3) was obtained by fitting a smooth curve through the fluorescence excitation spectrum and splicing this curve from 320 to 340 nm onto the original absorption spectrum from 220 to 320 nm.

A long-wavelength tail was also present in the absorption spectrum of tyrosine in aqueous buffer at pH 7.6 (Fig. 2 B, thin solid trace). The tyrosine tail is more complex than that of tryptophan, and includes two humps centered at ~295 and 340 nm. The extinction coefficients were over 100× smaller at these wavelengths than for the main peak at 275 nm, suggesting that one or both peaks may be due to an impurity. To test this idea, we measured the spectra of the dipeptides Tyr-Ala and Ala-Tyr in aqueous buffer at pH 7.6. We reasoned that the dipeptides are unlikely to contain the same impurities in the same amounts as tyrosine, yet should have a similar absorption spectrum to tyrosine, since they contain the same phenol chromophore as free tyrosine, and the alanine and peptide bond moieties have negligible absorption at wavelengths longer than 220 nm. The spectra of Tyr-Ala and tyrosine (Fig. 2 B) at pH 7.6 nearly superimposed at wavelengths shorter than 290 nm, indicating that incorporation into a dipeptide did not perturb the phenol chromophore significantly. No 340-nm peak was observed in Tyr-Ala, suggesting that this feature in the tyrosine spectrum was likely due to an impurity. The absorption at 295 nm, on the other hand, was only two times smaller in Tyr-Ala than in tyrosine, and most of this effect could be accounted for by the loss of the broad 340-nm feature, suggesting that the 295-nm feature is a real component of the tyrosine spectrum.

A small fraction of tyrosine should be present as the tyrosinate anion at pH 7.6, since the pK_a of the phenolic hydroxyl group of tyrosine is 10.1 (Creighton, 1993). If the hump at 295 nm is due to tyrosinate absorption, then lowering the pH should decrease its amplitude. Indeed, lowering the pH to 5.6 effectively eliminated the 295-nm peak in the Tyr-Ala spectrum (Fig. 2 B), identifying it as tyrosinate absorption. The residual tail at $\lambda > 300$ nm in the pH 5.6 spectrum is probably due to light scattering. The spectra of Ala-Tyr (not shown) and Tyr-Ala were indistinguishable at the same pH.

Fig. 3 shows the absorption spectra of tryptophan and Tyr-Ala from Fig. 2 as well as the spectra of the other near UV-absorbing protein chromophores phenylalanine, cystine, tyrosinate, and the thiolate anion of cysteine. The 293-nm absorption maximum of tyrosinate in Fig. 3 confirms the assignment of the 295-nm hump in the pH 7.6 spectra of tyrosine and Tyr-Ala (Fig. 2 B) to this species.

Action Spectra of UV-absorbing Amino Acids

This section derives a theoretical expression for computing the wavelength-dependent probability of photochemical modification (the action spectrum) of a UV-absorbing amino acid from the molecule's absorption spectrum and the spectrum of the exciting light. Fig. 9 (below) compares the action spectra estimated in this way for various UV-absorbing amino acids to the action spectrum of the UV effect on CNG channel currents.

The attenuation of light traveling through a system of homo-

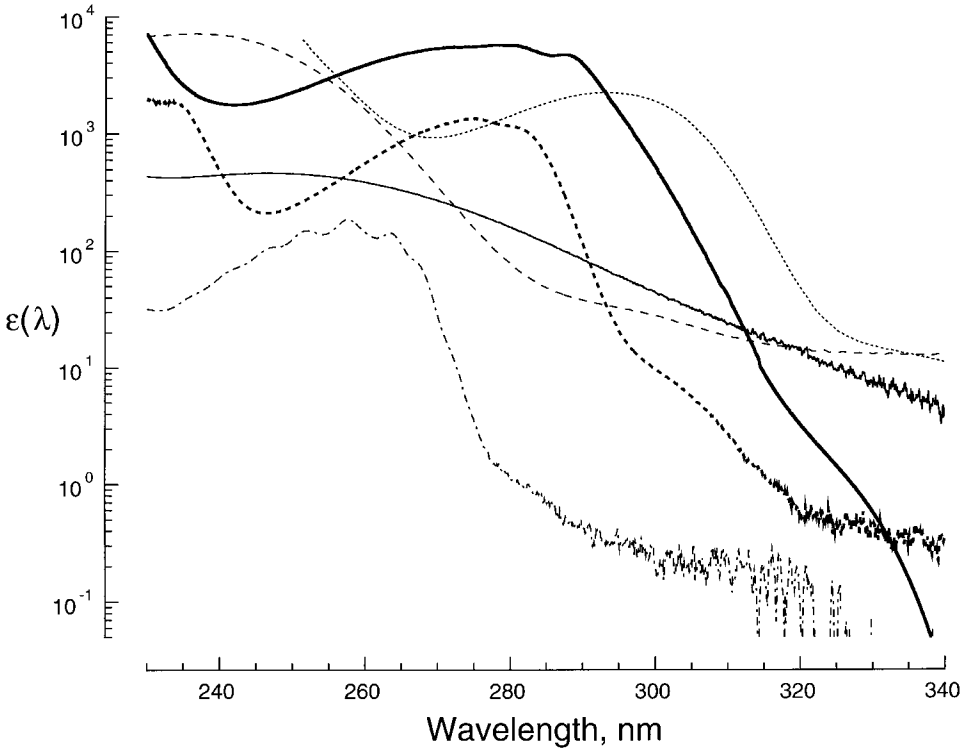

Figure 3. Absorption spectra of near-UV absorbing amino acids. Extinction coefficients ($M^{-1} \cdot cm^{-1}$) were computed from absorbance values using Beer's law (Eq. 44), and are plotted against wavelength on semi-logarithmic coordinates. The compounds, symbols, wavelengths of maximal near-UV absorption, λ_{max}, and extinction coefficients at λ_{max} are: tryptophan (solid bold line), 279.7 nm and 5,659; tyrosine (in the form of the dipeptide Tyr-Ala, pH 7.6, see materials and methods) (dashed bold line), 275.6 nm and 1,330; phenylalanine (dot-and-dashed line), 257.7 nm and 187, tyrosinate (ionized tyrosine formed by dissolving tyrosine in 100 mM NaOH) (short dashed line), 293.5 nm and 2,240; the thiolate form of cysteine (ionized cysteine formed by dissolving cysteine in 100 mM NaOH) (long dashed line), 237.1 nm and 7,146; and cystine (thin solid line), 247 nm and 465. All compounds except tyrosinate and the thiolate anion of cysteine were dissolved in the standard sodium solution described in materials and methods. Histidine, which also contains an extended pi electron system, does not absorb significantly at these wavelengths.

geneous, noninteracting absorbers is described by Beer's Law (Calvert and Pitts, 1966):

$$J_t = Je^{-\sigma bc}, \tag{1}$$

where J_t and J are the intensities of the transmitted and incident light, respectively, (quanta $\cdot$ cm^{-2} $\cdot$ s^{-1}), σ is the absorption cross section of the absorbing molecules (cm^2 $\cdot$ molecule^{-1}), b is the pathlength of the sample (cm), and c is the absorber concentration (molecules $\cdot$ cm^{-3}).

If the only transmission loss through the sample is due to light absorption, then:

$$J_a = J - J_t, \tag{2}$$

where J_a is the intensity of light absorbed by the sample. Combining Eqs. 1 and 2, the absorbed intensity is given by Eq. 3:

$$J_a = J(1 - e^{-\sigma bc}). \tag{3}$$

For an optically dilute sample (such as channel proteins in a membrane patch), σbc is much less than one, so that:

$$J_a = J\sigma bc. \tag{4}$$

In this limit, the probability of absorbing a photon, P_a, is the same for all of the absorbers in the sample, and is given by the ratio:

$$P_a = \frac{Q_a}{N_a}, \tag{5}$$

where Q_a is the total number of quanta absorbed by the sample and N_a is the number of absorbers in the sample. In a brief time interval dt, the number of absorbed quanta, dQ_a, is given by:

$$dQ_a = AJ_a dt, \tag{6}$$

where A is the cross-sectional area of the light beam (cm^2). After irradiation for a time τ (s), the total number of absorbed quanta is obtained by integrating Eq. 6:

$$Q_a = AJ\sigma bc\,\tau, \tag{7}$$

where use was made of Eq. 4. The number of absorbers in the illuminated volume is the absorber concentration multiplied by that volume:

$$N_a = Abc, \tag{8}$$

where the illuminated volume is $A \cdot b$. The probability of photon absorption by an individual chromophore is obtained by combining Eqs. 5, 7, and 8:

$$P_a = J\sigma\tau. \tag{9}$$

Let ϕ denote the (unitless) quantum yield, which is the fraction of absorptions that are followed by a photochemical transformation (Fig. 1). The probability that a chromophore will undergo photochemical modification, P_m, is then (Eq. 10):

$$P_m = J\sigma\phi\tau. \tag{10}$$

Since the absorption cross sections of the amino acids (Fig. 3) are constant to within 1% over the narrow bandwidth of the UV laser (0.01 nm FWHM), the excitation light in the experiments using the pulsed laser may be considered monochromatic. This approximation is not valid, however, for the much broader bandwidth light (10 nm FWHM) from the arc lamp. For those experiments, the probability of photochemical modification of an individual absorber is obtained by integrating Eq. 10 over all wavelengths:

$$P_m = \phi\tau\int_0^\infty J(\lambda)\sigma(\lambda)d\lambda, \tag{11}$$

where the wavelength dependence of J and σ is now shown explicitly. For simplicity, the quantum yield was assumed to be independent of wavelength and therefore removed from the integrand in Eq. 11. This is a reasonable approximation if absorption at different wavelengths populates the same excited electronic state. The intensity distribution of the exciting light reaching the preparation, $J(\lambda)$, is determined by the spectral output of the arc lamp, $L(\lambda)$, and the combined transmission spectrum $F(\lambda)$ of all optical filter(s) in the beam path:

$$J(\lambda) = L(\lambda)F(\lambda). \tag{12}$$

The total intensity of the excitation beam, J_{tot}, is the sum of these contributions at all wavelengths:

$$J_{tot} = \int_0^\infty L(\lambda)F(\lambda)d\lambda. \tag{13}$$

Defining $S_n(\lambda)$ as the normalized spectral distribution of the excitation light,

$$S_n(\lambda) = [L(\lambda)F(\lambda)]/J_{tot}, \tag{14}$$

P_m is obtained by substituting Eqs. 12–14 into Eq. 11:

$$P_m = \phi\tau J_{tot}\int_0^\infty \sigma(\lambda)S_n(\lambda)d\lambda. \tag{15}$$

All of the factors on the right-hand side of Eq. 15 except the quantum yield ϕ were measured directly. The total light intensity at the sample, J_{tot}, was obtained by the calibration procedure described above. The factor $S_n(\lambda)$ was obtained using Eq. 14 as follows. For a given set of optical filters, the combined transmission spectrum, $F(\lambda)$, was computed from the product of the transmission spectra of the filters in the beam, which were measured individually in a spectrophotometer. The spectral output of the xenon arc lamp, $L(\lambda)$, was measured using calibrated interference filters and a calibrated radiometer, and agreed with the manufacturer's published spectrum. The product $F(\lambda) \cdot L(\lambda)$ was then divided by its integral over all wavelengths, ensuring that $S_n(\lambda)$ obeyed the normalization condition (Eq. 16):

$$\int_0^\infty S_n(\lambda)d\lambda = 1. \tag{16}$$

The wavelength-dependent absorption cross sections, $\sigma(\lambda)$ (μm^2) were obtained from the corresponding extinction coefficients, $\epsilon(\lambda)$, in molar^{-1} $\cdot$ cm^{-1} (Figs. 2 and 3) using the relation $\sigma(\lambda) = \epsilon(\lambda) \cdot 3.83 \times 10^{-13}$. The wavelength-dependent photochemical modification probability for each of the UV-absorbing amino acids in Fig. 3 was then computed using Eq. 15 (assuming a wavelength-independent quantum yield for each compound).

One- and Multi-Photon Photochemistry

The wavelength dependence of the absorption probability (Eq. 9) was derived in the previous section starting with the Lambert-Beer law (Eq. 1). The latter applies only to so-called one-photon absorption processes, in which a chromophore is excited by the absorption of a single photon. A generalized form of Eq. 9 that accounts for absorption by higher-order mechanisms is (Yariv, 1975; Steinfeld, 1985):

$$P_a(r) = \sum_{r=0}^{\infty} J^r \sigma_r \tau. \tag{17}$$

In Eq. 17, $P_a(r)$ denotes the probability of photoexcitation by absorption of r photons simultaneously, and σ_r denotes the r-photon absorption cross section [$cm^{(2r)} \cdot s^{(r-1)}$]. The steep power-law dependence of the absorption probability on the incident light intensity may be used to determine the mechanism of light absorption in a photochemical modification experiment. For an r-photon absorption process, the probabilities of exciting a chromophore using lights of different intensities (denoted J_{hi} and J_{lo}), are equal if the corresponding exposure durations (denoted τ_{hi} and τ_{lo}) are related by:

$$\frac{\tau_{lo}}{\tau_{hi}} = \left[\frac{J_{hi}(\lambda)}{J_{lo}(\lambda)}\right]^r. \tag{18}$$

For the special case of a one-photon absorption mechanism, the absorption probability depends only on the total photon dose D, since $D = J \cdot \tau$.

theory

UV Dose–Response Relation

This section develops a quantitative theory for the dose dependence of CNG channel macroscopic currents. Several models for the effects of photochemical modification on channel function are considered, and equations for the UV dose–response relation are derived for each model.

Assume that the channels contain n identical target residues per channel subunit. (Target residues are defined as the amino acids whose UV modification changes the channel current.) Since photochemical modification of the targets occurs randomly, irradiation transforms a patch of N initially identical channels into a complex mixture containing channel subpopulations with different sets of modified targets. The macroscopic current I after exposure to a photon dose D is the sum of the currents through all channel subpopulations. Assume that the effect of UV on the current through any channel depends only on k, the total number of modified targets in that channel. The dose dependence of the patch current is then:

$$I(D) = \sum_{k=0}^{4n} N(k, D) i_{sc}(k) P_o(k), \tag{19}$$

where $N(k,D)$ is the number of channels with k modified targets after a UV dose D [$0 \le N(k,D) \le N$], and $i_{sc}(k)$ and $P_o(k)$ are the single channel current and open probability of channels with k modified targets, respectively. The summation index in Eq. 19 ranges from 0 to $4n$ because the channels are assumed to assemble as tetramers (Liu et al., 1996; Morrill and MacKinnon, 1999). The $N(k,D)$ obey the restriction (Eq. 20):

$$\sum_{k=0}^{4n} N(k, D) = N \tag{20}$$

for all values of D, reflecting the assumption that UV does not "destroy" channels. (As discussed below, functional destruction of a channel is accounted for by setting the product of its unitary current and open probability to zero).

If the photochemical modifications occur independently, then the fraction of channels f containing a total of k modified targets after a dose D is given by the Bernoulli distribution (see, for example, DeFelice, 1981):

$$f(k, D) = \binom{4n}{k} [1 - \exp(-\sigma\phi D)]^k [\exp(-\sigma\phi D)]^{(4n-k)}, \tag{21}$$

where $0 \le f(k,D) \le 1$. The first term on the right side of Eq. 21 is the appropriate binomial coefficient, while the exponential terms in brackets represent the probabilities that an individual target is or is not modified, respectively. Before irradiation (Eq. 22),

$$\lim_{D \to 0} f(k, D) = \begin{cases} 0; & k > 0 \\ 1; & k = 0 \end{cases}. \tag{22}$$

The number of modified targets increases with UV dose until, after an arbitrarily large dose (Eq. 23),

$$\lim_{D \to \infty} f(k, D) = \begin{cases} 1; & k = 4n \\ 0; & k < 4n \end{cases}. \tag{23}$$

Using Eq. 19 and the identity (Eq. 24)

$$f(k, D) = \frac{N(k, D)}{N}, \tag{24}$$

the fraction of current remaining as a function of dose is

$$\frac{I(D)}{I(0)} = \sum_{k=0}^{4n} f(k, D) \frac{i_{sc}(k) P_o(k)}{i_{sc}(0) P_o(0)}. \tag{25}$$

In this formalism, the dose dependence of the UV effect is contained entirely in the $f(k,D)$ factors.

The following sections describe three possible physical models for the effect of UV on CNG channels activated by saturating concentrations of ligand. "Rules" are given for each model that specify the effect of each target modification on the channels' unitary current, $i_{sc}(k)$, and open probability, $P_o(k)$. The dose dependence of the channel current is obtained by combining these rules with Eq. 25.

Independent, "All-or-None" Model

Suppose that photochemical modification of a channel's UV targets has no effect on the current until alteration of a critical number of targets (denoted n^*) renders the channel nonconducting. This model does not identify whether UV alters the channels' unitary current or open probability. However, their product is given by:

$$i_{sc}(k) P_o(k) = \begin{cases} 0; & k \ge n^* \\ i_{sc}(0) P_o(0); & k < n^* \end{cases}. \tag{26}$$

The UV dose–response relation obtained by combining Eqs. 25 and Eq. 26 is:

$$\frac{I(D)}{I(0)} = 1 - \sum_{k=n^*}^{4n} f(k, D). \tag{27}$$

In the limit that all of the targets must be modified to produce the all-or-none effect (i.e., $n^* = 4n$), Eq. 27 simplifies to:

$$\frac{I(D)}{I(0)} = 1 - [1 - \exp(-\sigma\phi D)]^{n^*}. \quad (28)$$

In the opposite limit that modification of a single target abolishes the channel current (i.e., $n^* = 1$), Eq. 27 reduces to single exponential form (Eq. 29):

$$\frac{I(D)}{I(0)} = \exp(-4n\sigma\phi D). \quad (29)$$

Proportional Conductance Model

Suppose that each target modification reduces a channel's unitary conductance by an equivalent amount without affecting its open probability, and that the current through a single open channel is reduced to zero after all of the targets are modified. Then (Eqs. 30 and 31):

$$i_{sc}(k) = i_{sc}(0)\left(\frac{4n-k}{4n}\right);\ 0 \le k \le 4n \quad (30)$$

and

$$P_o(k) = P_o(0);\ 0 \le k \le 4n. \quad (31)$$

The UV dose–response relation (Eq. 25) in this case reduces to

$$\frac{I(D)}{I(0)} = 1 - \sum_{k=0}^{4n} f(k, D)\frac{k}{4n}. \quad (32)$$

Evaluation of Eq. 32 yields the unexpected result:

$$\frac{I(D)}{I(0)} = \exp(-\sigma\phi D); \quad (33)$$

i.e., the UV dose–response relation is a single exponential function and does not depend on the total number of targets.

Energy Additive Model

Assume that modification of the UV targets does not affect the single channel current,

$$i_{sc}(k) = i_{sc}(0);\ 0 \le k \le 4n, \quad (34)$$

but instead reduces the macroscopic current by lowering the channels' open probability. The dependence of P_o on k is complex and is derived as follows. First, assume that each subpopulation of fully liganded channels with k modified targets has a single closed state (denoted C_k) in equilibrium with a single open state (denoted O_k):

$$C_k \overset{K(k)}{\leftrightarrow} O_k,$$

where the equilibrium constant $K(k) = [O_k]/[C_k]$. Many cyclic allosteric models that are used to describe CNG channel activation reduce to a two-state system when ligand is present at saturating concentration (Monod et al., 1965; Liu et al., 1998). The equilibrium constant is related to the open probability by the relation:

$$P_o(k) = \frac{K(k)}{1 + K(k)}, \quad (35)$$

and to the standard free energy difference between O_k and C_k, $\Delta G^0(k)$, by the relation:

$$K(k) = \exp[-\Delta G^0(k)]. \quad (36)$$

In Eq. 36, the equilibrium constant is expressed in RT units, where R is the gas constant and T is the absolute temperature. The UV effect on channel current is modeled by assuming that the modification of k targets alters the free energy difference between the channels' open and closed states by a factor $\Delta\Delta G^0(k)$. The reduction in channel current by UV (see below) implies that $\Delta\Delta G^0(k)$ is unfavorable (i.e., positive) and thus represents the free energy "cost" of modifying k targets. If $\Delta\Delta G^0(k)$ is assumed to be independent of $\Delta G^0(0)$, the free energy difference between the channels' open and closed states before irradiation, then $\Delta G^0(k)$ is equal to the sum:

$$\Delta G^0(k) = \Delta G^0(0) + \Delta\Delta G^0(k). \quad (37)$$

If the targets are assumed to be identical and independent, then the free energy costs associated with their modification will be equal and additive, so that:

$$\Delta\Delta G^0(k) = k\,\Delta\Delta G^0(1). \quad (38)$$

Combining Eqs. 35–38 yields the desired expression for $P_o(k)$:

$$P_o(k) = \frac{P_o(0)}{P_o(0) + [1 - P_o(0)]\exp[k\,\Delta\Delta G^0(1)]};\ 0 \le k \le 4n. \quad (39)$$

The UV dose–response relation is obtained by substituting Eqs. 34 and 39 into Eq. 25:

$$\frac{I(D)}{I(0)} = \sum_{k=0}^{4n} f(k, D)\frac{1 + \exp[\Delta G^0(0)]}{1 + \exp[\Delta G^0(0) + k \cdot \Delta\Delta G^0(1)]}. \quad (40)$$

RESULTS

Effect of UV Light on Uninjected Oocytes

Because UV light changed the conductance of patches from oocytes lacking exogenously expressed channels, it was necessary to characterize this effect before studying the effect of UV on CNG channels. For example, Fig. 4 A shows that the small initial leak current (23 pA at +50 mV) through a patch excised from an uninjected oocyte increased slightly after three equivalent doses of 1.08×10^{10} photons $\cdot\ \mu m^{-2}$ at 280 nm, but then increased rapidly after additional exposures, reaching 1,824 pA after a cumulative dose of 5.41×10^{10} photons $\cdot\ \mu m^{-2}$.

Two properties of this current suggested that it represented a UV-activated membrane conductance rather than an increased leakage current due to deterioration of the seal between the pipet wall and the oocyte membrane. First, as shown in Fig. 4 B, the current in symmetrical sodium solutions was 15% smaller at +70 than at −70 mV. The current–voltage relation for this patch (Fig. 4 C) demonstrates the inward rectification more clearly. Although the extent of the inward rectification varied between patches, it was observed in all experiments. The leakage current through the seal resistance is not expected to rectify in this manner. The UV-acti-

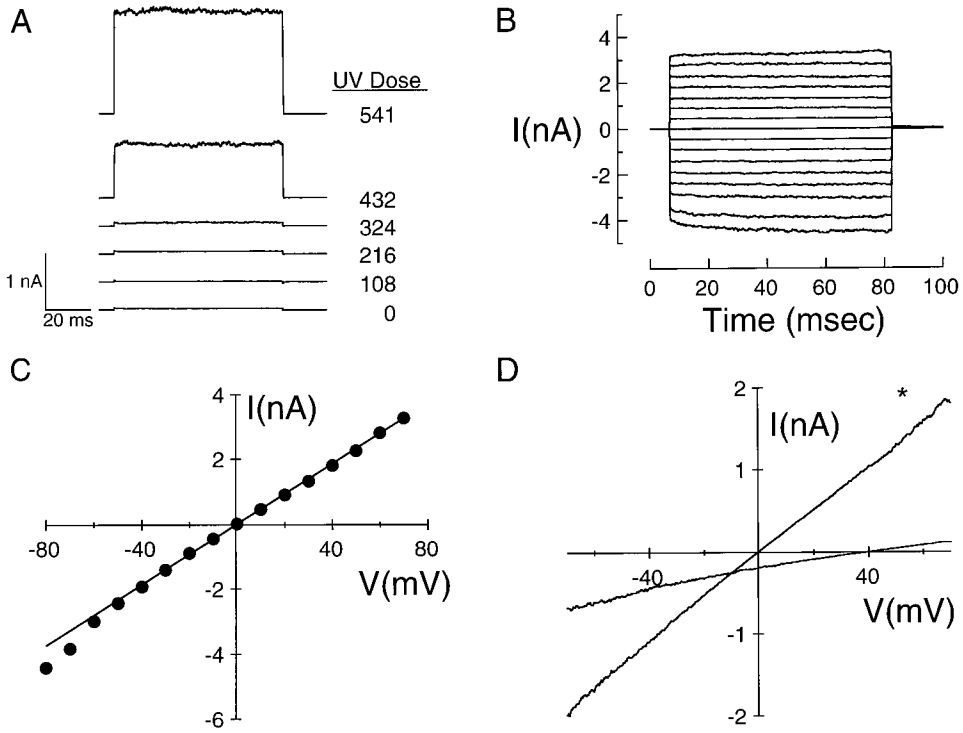

Figure 4. Characterization of UV-activated conductance in *Xenopus* oocytes. (A) UV effect on the current through an excised, inside-out patch from an uninjected oocyte in response to a 0–50-mV voltage step. UV doses (in photons $\times 10^8 \cdot \mu m^{-2}$) are indicated. The patch was irradiated in the absence of cGMP while held at 0 mV. (B) Voltage dependence of UV-activated conductance. Results for patch from A after exposure to 5.41×10^{10} photons $\cdot \mu m^{-2}$. Currents were elicited by stepping the patch from a holding potential of 0 mV to voltages from −80 to +70 mV in 10-mV increments. (C) Current–voltage relation (●) for the results in B. The fit is a straight line with slope 4.6×10^{-8} S. (D) Cation selectivity of UV-activated conductance. Currents were elicited by voltage ramps from −75 to +75 mV in 500 ms after exposing the patch to 1.78×10^{10} photons $\cdot \mu m^{-2}$. The trace indicated by * was obtained in symmetric 130-mM NaCl solutions; the other trace was obtained with 130 mM NaCl in the pipet and 26 mM NaCl in the bath. Voltages were not corrected for junction potentials. The results are from a different patch than that used in A–C. The currents in A–D were corrected for leak through the seal resistance by subtracting the current before irradiation.

vated conductance also exhibited ion selectivity. The voltage ramps in Fig. 4 D were applied in symmetrical 130-mM NaCl solutions (*) or with 130 and 26 mM NaCl in the pipet and bath solutions, respectively. In the latter configuration, the Nernst potentials for Na^+ and Cl^- are +40 and −40 mV, respectively. The patch current reversed sign at 42.1 mV, indicating that the conductance was strongly selective for cations over anions. Before irradiation, the seal leakage conductance did not exhibit ion selectivity. Taken together, these results suggest that the large currents induced by irradiation of uninjected oocyte patches passed through UV-activated conductance sites.

The markedly nonlinear current–dose (I-D) relations for the UV-activated conductances from nine separate patches are illustrated in Fig. 5 A. The slopes of the curves and their positions on the dose axis varied as expected if the patches contained different numbers of UV-activated conductance sites. It should be possible to correct for this difference in scaling by normalizing the results for different patches. However, all attempts to measure the maximal UV-activated current directly were unsuccessful because the current amplitudes invariably exceeded the saturation limit of the patch-clamp amplifier. Moreover, the leak currents after large UV doses were often unstable and sometimes drifted in a time-dependent manner. Lacking a direct estimate for the limiting current amplitude, we analyzed the unnormalized I-D relations using a variant of the all-or-none model described above. Assume that there are N identical, initially dormant UV-activated conductances in a patch, and that activation of a site occurs in an all-or-none fashion upon modification of a critical number (n^*) of UV targets in the conductance. The product of the unitary current and open probability of a site containing k modified targets is then (Eq. 41):

$$i_{sc}(k)P_o(k) = \begin{cases} i_{sc}(n^*)P_o(n^*);\ k \geq n^* \\ 0;\ k < n^* \end{cases}. \qquad (41)$$

The current through a patch containing many sites is given by:

$$I(D) = N\, i_{sc}(n^*)P_o(n^*)[1 - \exp(-\sigma\phi D)]^{n^*}. \qquad (42)$$

The form of Eq. 42 suggests that the I-D curves for patches containing different numbers of UV-activated conductances should be the same, save for a vertical displacement, when plotted on double logarithmic coordinates. Indeed, the shapes of the relations were similar when displayed in this manner (Fig. 5 B). The invariant shape of the relations is more apparent when the results in Fig. 5 B are shifted vertically to correct for differences in the number of UV-activated conductance

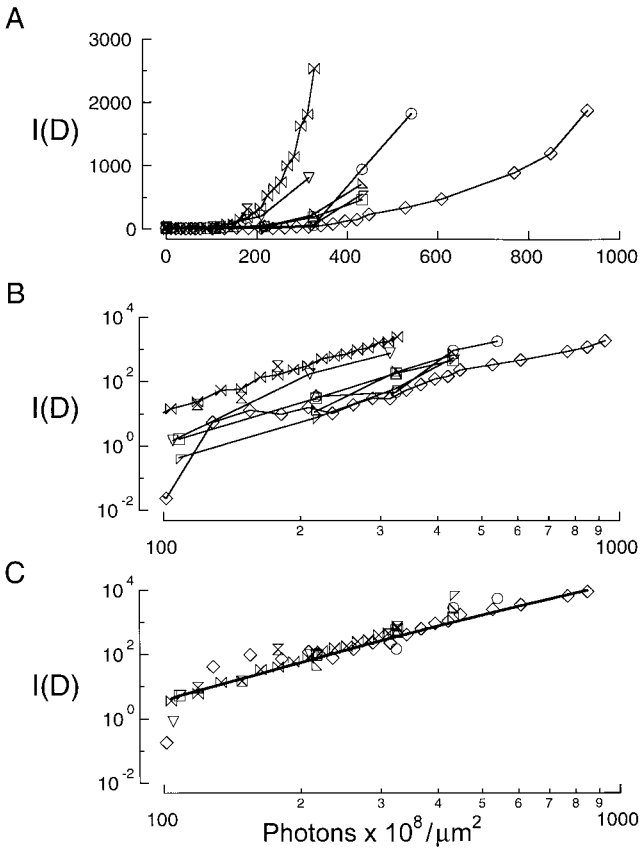

Figure 5. Dose dependence of UV-activated conductance. (A) UV dose–response relations for UV-activated conductances from nine patches. The total patch current in picoamperes is plotted as a function of the cumulative photon dose. Different symbols indicate separate experiments. Patches were irradiated while held at 0 mV and currents were recorded at +50 mV. The bath and pipet contained standard sodium solution with no cGMP (see materials and methods). (B) Results from A, plotted on double logarithmic coordinates. (C) Same as B, except the results from each experiment were shifted along the ordinate to correct for the difference in current amplitudes at 3×10^{10} photons $\cdot \mu m^{-2}$. The solid line is a fit to the combined results using the modified all-or-none model (Eq. 42) with the target number n^* equal to 4.3 ± 0.5. Currents in A–D were corrected for leak through the seal resistance by subtracting the current before irradiation.

sites per patch (Fig. 5 C). The target number obtained from the fit to the combined results using Eq. 42 (solid curve) indicates that each UV-activated conductance site is activated after UV modification of about four or five targets. The quantum yield for modification of the targets in the UV-activated conductance was estimated from a second fitting parameter, which is equal to the product $\sigma \cdot \phi$. Since the nature of the target residues is unknown, multiple estimates for ϕ were made using the known cross sections (σ) of various UV-absorbing amino acids (Fig. 3). The quantum yields were 0.0028 ± 0.0007 for tryptophan targets and 0.014 ± 0.003 for tyrosine targets. These values are comparable with the photochemical quantum yields of these amino acids obtained from UV photolysis studies of various globular proteins (McLaren and Shugar, 1964; Vladimirov et al., 1970; Grossweiner, 1976).

We were unable to identify pharmacological blockers of the UV-activated conductance. However, other experiments (not shown) indicated that these sites are not affected by cGMP at concentrations up to 1 mM. Since the currents through CNG channels were obtained as the difference between currents in the presence and absence of cGMP, the UV-activated conductance did not interfere with our measurements of UV effects on CNG channel currents.

Possible interference from the UV-activated conductance might also be avoided by carrying out the UV-modification experiments in cells other than *Xenopus* oocytes. However, possibly related UV-activated conductances have been reported in a variety of mammalian cell lines (Mendez and Penner, 1998; Hsu et al., 1999; Wang et al., 1999), suggesting that the sites may originate from a component present in many biological membranes. The apparently ubiquitous distribution of the UV-activated conductances underscores the need for caution to avoid possible artifacts in channel experiments that use UV light.

Effect of UV Light on CNG Channel Currents

We assessed the functional effects of UV light on CNG channels by comparing the amplitudes of currents through inside-out membrane patches expressing RET channels before and after irradiation. Patches were rejected for further use if the cGMP-dependent current amplitude varied more than ±5% before UV. Unless otherwise noted, due to the strong absorption of cGMP in the near UV (ϵ_{max} = 14,167 $M^{-1} \cdot cm^{-1}$ at λ_{max} = 253.5 nm, this work), patches were irradiated in the absence of ligand to prevent photochemical modification of cGMP or its cross linking to the channels.

Fig. 6 A shows results from a typical experiment. Each UV exposure decreased the cGMP-dependent outward current, as shown by the solid traces with successively smaller amplitudes. The amplitude of the cGMP-activated current, I, normalized by its value before irradiation, I_0, is shown as a function of time for this patch in Fig. 6 B. ○ and ●, respectively, indicate trials that were or were not immediately preceded by a UV exposure. The current amplitude decreased in a dose-dependent manner, reaching 34% of its initial value after a cumulative dose of 5.1×10^9 photons $\cdot \mu m^{-2}$ (corresponding to the 11th ○). The amplitude of this residual current remained constant for the next 48 min in the absence of additional UV, ruling out light-independent mechanisms for the rundown. The irreversibility of the current is consistent with a mechanism in which UV transforms channel residues into stable, covalently modified products (Fig. 1).

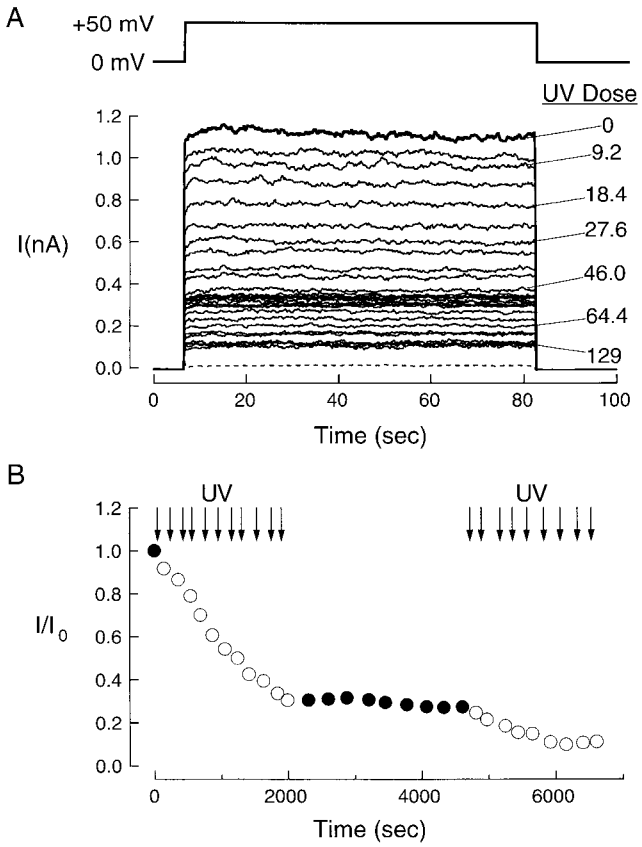

Figure 6. Effect of UV light on CNG channel currents. (A) Ionic currents before and after UV exposure. The currents were recorded in symmetrical 130-mM NaCl from an excised, inside-out membrane patch from a *Xenopus* oocyte membrane expressing bovine rod CNG (RET) channels. The template at top shows the timing of the voltage step. The bold trace at top is the current in the presence of 100 μM (approximately half-saturating) intracellular cGMP before UV exposure. The solid traces of successively smaller amplitude were obtained after increasing cumulative UV exposures. UV doses (in photons $\times 10^8 \cdot \mu m^{-2}$) are indicated for selected traces. The patch was irradiated with light from a xenon arc lamp (280 nm) in the absence of cGMP. The light intensity was 4.6×10^8 photons μm^{-2} s^{-1}. The cyclic GMP-activated currents were corrected for leak by subtracting the current in the absence of cGMP after the same dose. The dashed trace shows the leak current before irradiation. The initial cGMP-activated current was 1,120 pA; the current at the end of the experiment (after a cumulative dose of 1.3×10^{10} photons $\cdot \mu m^{-2}$) was 125 pA. (B) Light and time dependence of currents. The channel current (I), normalized by the current before UV exposure (I_0), is plotted as a function of time during the experiment. Each open symbol represents the current recorded after a 1-s exposure containing 4.6×10^8 photons $\cdot \mu m^{-2}$ except for the last two open symbols, which were recorded after 5-s exposures that each contained 2.3×10^9 photons $\cdot \mu m^{-2}$. Closed symbols denote currents recorded with no intervening UV exposure. Arrows indicate timing of UV applications. Results are from patch in A.

The last two UV doses for the experiment shown in Fig. 6 did not reduce the cGMP-activated current significantly; however, the leak current at this point was much larger than the cGMP-activated current (probably due to the contribution of the UV-activated conductance, see above). Such large, unstable leak currents were observed in most patches before rupture, and prevented an accurate determination of the limiting current amplitude. The leak current for some patches was smaller in proportion to the cGMP-activated currents (perhaps due to a relatively small ratio of UV-activated conductance sites to CNG channels). These results provided an upper bound of ~5% for the limiting value of I/I_0.

Strategy for Identifying Target Residues

What are the nature, number, and location of the target amino acid(s) in CNG channels? In principle, modification of any channel residue might alter the current amplitude. We used UV wavelengths longer than 240 nm to restrict the possible UV targets to a small subset of the channel residues. The only amino acids that absorb in this region of the spectrum are tryptophan, tyrosine, phenylalanine, cysteine, and cystine (Fig. 3). The identity of the target(s) was narrowed further by comparing the wavelength dependence of the UV effect (the action spectrum) to the wavelength dependence of the absorption probability (the absorption spectrum) of each candidate target amino acid (see Figs. 8–10). Mutagenesis was also used in an effort to identify individual target residues in the channel sequence (see Fig. 12).

Intensity Dependence

The strategy outlined above uses the distinct absorption spectra of the amino acids (Fig. 3) as "fingerprints" to identify the UV targets in CNG channels. The light used in the channel photochemical modification experiments (Fig. 6) was much more intense than the weak light used to probe the absorption of the amino acids (Figs. 2 and 3), raising the possibility that some of the channel targets were modified after simultaneous absorption of multiple photons. Our absorption spectra, however, measure single-photon absorptions exclusively. Since the one-photon and higher-order absorption spectra of a given chromophore may differ radically (Callomon et al., 1966; Goodman and Rava, 1983; Maiti et al., 1997), our strategy for identifying the UV targets in the channels will work only if the targets are modified after absorption by a one-photon mechanism. We examined the intensity dependence of the UV effect on CNG channels to determine the photochemical mechanism of light absorption by the channel targets.

Fig. 7, A and B, compares the currents through RET channels irradiated with UV from a continuous arc lamp source (λ = 280 nm) or from a much more intense pulsed UV laser (λ = 266 nm). Each panel displays collected results from many experiments as UV dose–response relations, which plot the cGMP-activated current, normalized by its pre-UV amplitude,

against the logarithm of the cumulative photon dose. Results from independent experiments at each light intensity were pooled by a two-part procedure. The results from each experiment were fit with the simplified version of the "all-or-none" model (Eq. 28), in order to estimate $D_{1/2}$, the UV dose that reduced the current to half of its initial amplitude. Each set of points was then shifted along the abscissa so that the $D_{1/2}$ for the shifted results was equal to the average $D_{1/2}$ of the unshifted results for all experiments at similar light intensities. The shifted results allowed a better comparison of the shapes of the UV dose–response relations than the unshifted points. Since the fits were used only to characterize the slopes of the curves and their positions on the abscissa, the validity of conclusions drawn from comparisons of these parameters are independent of the correctness of the all-or-none model.

The UV dose–response relations for channels irradiated with low- and high-intensity UV were strikingly similar, despite the eight order of magnitude difference in light intensities. The similarity in the $D_{1/2}$ values indicates that the UV effect depended only on the total photon dose, and not on the rate at which photons were delivered to the patches. This finding is consistent with absorption by a one-photon absorption mechanism, but not two-photon or higher-order mechanisms. The small difference between the wavelengths of the two light sources has only a slight (<7%) effect on the channels' UV sensitivity (see Figs. 8 and 9, below). The maximal slopes of the relations were also similar for low- and high-intensity irradiation, suggesting that the nature and relative amounts of the various photoproducts formed were independent of light intensity.

The results for low-intensity UV were obtained by irradiating the channels in the absence of cGMP, while those for high-intensity UV were obtained by irradiating the channels in the presence of a half-saturating concentration of cGMP (100 μM). However, similar results were obtained for channels irradiated with high-intensity UV in the absence of cGMP, indicating that

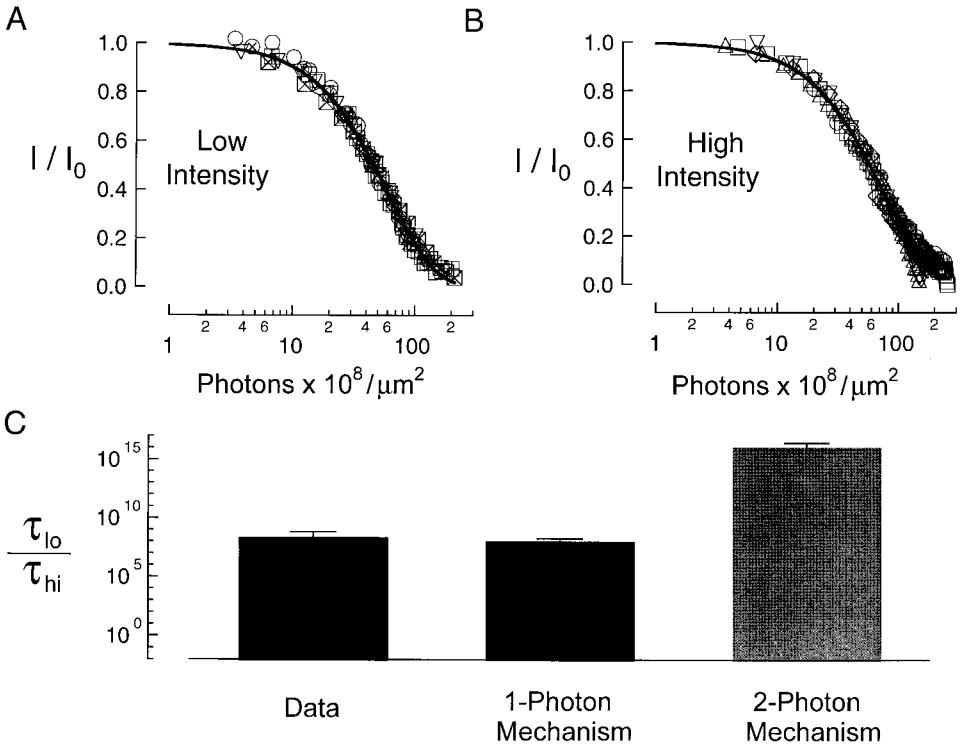

Figure 7. Evidence that the UV effect involves a one-photon absorption mechanism. (A and B) UV dose dependence of currents through RET channels. Patches were irradiated with a low-intensity continuous xenon arc lamp (λ = 280 nm, six patches, A) or a high-intensity pulsed UV laser (λ = 266 nm, six patches, B). Different symbols indicate separate experiments. To facilitate comparison of the shapes of the curves, results from each experiment were shifted along the abscissa so that the $D_{1/2}$ value was equal to its average value for the unshifted results for all experiments at similar light intensities. The $D_{1/2}$ values for the unshifted results ranged from 3.18 to 5.23 × 10^9 photons · μm^{-2}, with an average of (3.84 ± 0.39) × 10^9 photons · μm^{-2} (mean ± SEM) for low-intensity excitation, and from 3.2 to 8.4 × 10^9 photons · μm^{-2}, with a mean of (4.68 ± 0.78) × 10^9 photons · μm^{-2} for high-intensity excitation. The smooth curve in each panel is a fit to the collected results using Eq. 28 of the text. The fitting parameter n^*, which provides a measure of the maximum steepness of the relation, was equal to 1.21 ± 0.05 (mean ± SD) and 1.33 ± 0.03, respectively, for the results in A and B. Currents in A were recorded in 100 μM cGMP after irradiating the patches in the absence of cGMP. Currents in B were measured in 100 μM cGMP after irradiating the patches in the presence of 100 μM cGMP. The arc lamp intensities ranged (0.32–1.5) × 10^8 photons · μm^{-2} · s^{-1} for different experiments; the laser intensities ranged (2.1–3.9) × 10^{16} photons · μm^{-2} · s^{-1}, and were corrected for attenuation by cGMP in the bath solution. (C) Comparison of the UV effect at low- and high-light intensities with predictions for one- and two-photon absorption mechanisms. The ordinate is the ratio of τ_{lo} to τ_{hi}, where τ_{lo} and τ_{hi} are the average UV exposure times required to reduce the current to half of its maximal (pre-UV) amplitude following low- or high-intensity irradiation, respectively. The ratio τ_{lo} / τ_{hi} computed from the results in A and B was 2.32 × 10^8. The theoretical ratios were calculated using Eq. 18 and were 1.09 × 10^8 and 1.20 × 10^{16} for one- and two-photon absorption mechanisms, respectively. The slight difference in UV wavelengths used in A (280 nm) and B (266 nm) has a minimal effect (<7%) on the channels' UV sensitivity (see Fig. 9).

the effect of UV was not dependent on the activation state of the channels. For high-intensity UV, we confined the analysis to results on channels irradiated in the presence of cGMP, due to the much larger number of experiments performed under those conditions.

The $D_{1/2}$ values for the results in Fig. 7, A and B, were converted into $\tau_{1/2}$ values (the exposure times required for 50% current reduction) using the relation (Eq. 43):

$$\tau_{1/2} = D_{1/2}/J, \tag{43}$$

and the ratio of $\tau_{1/2}$ values is shown in Fig. 7 C ("data"). This ratio is compared with the predicted $\tau_{1/2}$ ratios computed from Eq. 18 for one- and two-photon absorption mechanisms. The J_{lo} and J_{hi} factors in Eq. 18 were obtained from the average light intensities used in the low-intensity (Fig. 7 A) and high-intensity (B) experiments, respectively. The experimental $\tau_{1/2}$ ratio was similar to the predicted ratio for a one-photon absorption mechanism, but was ~8 log units smaller than the ratio for absorption by a two-photon mechanism. (The $\tau_{1/2}$ ratios predicted for three-photon and higher-order absorption mechanisms were even larger.) This analysis indicates conclusively that UV modification of the target residue(s) in the channels followed absorption by a one-photon mechanism, and validates the strategy outlined above for identifying the channel targets.

Wavelength Dependence

Fig. 8 shows the wavelength dependence of the UV effect on currents through RET channels activated by saturating cGMP. The spectral width of the exciting light in each experiment was ~10 nm FWHM, and the range of peak wavelengths employed (250–330 nm) spanned the lowest energy one-photon absorption bands of all possible target amino acids (Fig. 3). UV decreased the channel currents in a dose-dependent manner at all wavelengths studied. The efficacy of photons of different wavelengths varied greatly, however, as evidenced by the large variations in the horizontal positions of the corresponding UV dose–response relations.

Slope factors and $D_{1/2}$ values were obtained by fitting the relations with Eq. 28. On a quantal basis, 280-nm photons were most effective, with $D_{1/2} = (4.6 \pm 0.3) \times 10^9$ photons $\cdot$ μm^{-2} (mean $\pm$ SEM). Photon efficiencies fell off asymmetrically about the maximum at 280 nm: $D_{1/2}$ was 74-fold larger at 310 nm compared with 280 nm, but only 1.5-fold larger at 250 nm than at 280 nm. Photons of 330-nm wavelength, the longest tested, were 500× less effective than 280-nm photons.

Fig. 9 A plots the channels' UV sensitivity (defined as the reciprocal of $D_{1/2}$) as a function of wavelength. Also shown are the predicted action spectra for tryptophan and tyrosine targets, computed from the corresponding absorption spectra using Eq. 15. The predicted action spectra differed from the corresponding absorption spectra due to corrections for the finite bandwidth of the exciting light and for wavelength-dependent variations in the lamp intensity. The magnitude of these corrections (see materials and methods) were largest at the wavelengths with the steepest absorption slopes. For tryptophan, the correction procedure increased the absorption probability at 280 nm relative to

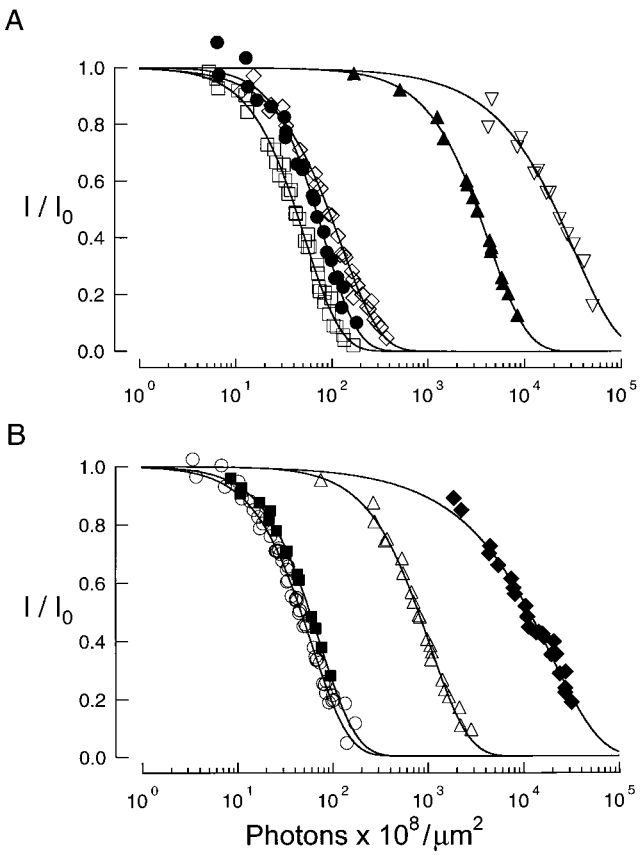

Figure 8. UV dose–response relations of RET channels irradiated at different wavelengths. (A) The channel current amplitude in saturating (1 mM) cGMP, I, normalized by the pre-UV amplitude, I_0, is plotted as a function of UV dose on semilogarithmic coordinates. Each type of symbol represents collected results from 3–10 separate patches at a given wavelength. The UV dose that reduced the current to half of its initial value, $D_{1/2}$, was estimated from fits to the results for each experiment using Eq. 28. To facilitate comparison of the shapes of the relations, the results from each experiment were shifted along the abscissa so that $D_{1/2}$ was equal to the average $D_{1/2}$ of the unshifted results for all experiments at the same wavelength. Smooth curves are fits to the collected results at each wavelength using Eq. 28. The excitation wavelengths, symbols, and number of experiments were: 250 nm (●), 3; 270 nm (□), 4; 290 nm (◇), 3; 310 nm (▲), 3; and 330 nm (▽), 2. The light source was a xenon arc lamp; light intensities ranged from 1.3×10^7 to 2.7×10^9 photons $\cdot$ $\mu m^{-2} \cdot s^{-1}$. Currents through channels activated by 1 mM (saturating) cGMP were recorded at +50 mV. Cyclic GMP was absent during irradiation. (B) Same as A, except the wavelengths, symbols, and number of experiments were: 260 nm (■), 3; 280 nm (○), 10; 300 nm (△), 4; and 320 nm (◆), 4.

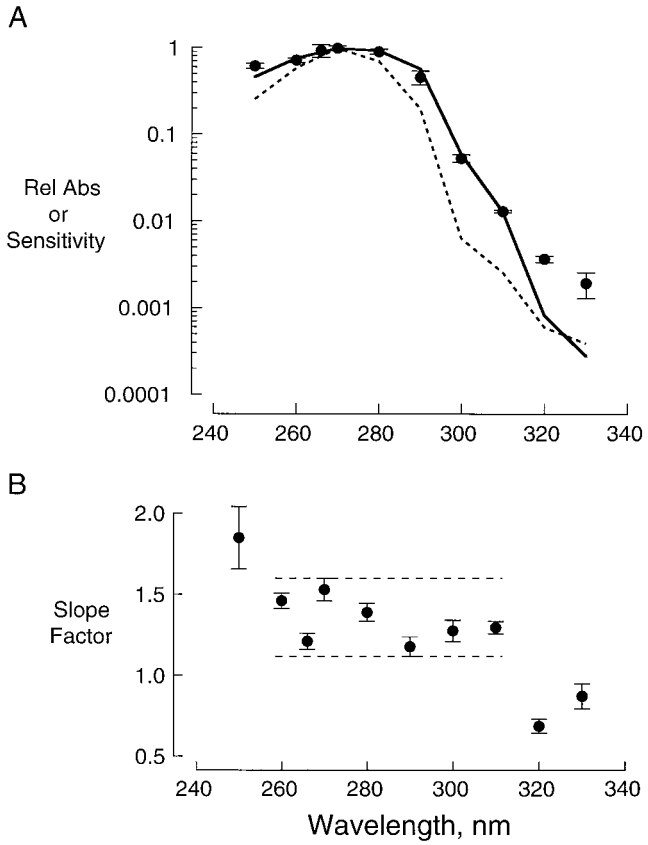

Figure 9. Wavelength dependence of UV sensitivity of CNG channels. (A) Action spectrum of UV effect compared with wavelength dependence of tryptophan and tyrosine absorption. The UV sensitivity at each excitation wavelength λ, defined as the reciprocal of $D_{1/2}(\lambda)$, was obtained from the fits in Fig. 8. Also shown is the UV sensitivity at 266 nm, obtained from the results in Fig. 7 B. The UV sensitivity (●, mean ± SEM), normalized to a value of 1.0 at 270 nm, is plotted as a function of wavelength on semilogarithmic coordinates. The predicted action spectra for photochemical modification of tryptophan (solid line) and tyrosine (dotted line) targets were calculated from their absorption spectra (Fig. 3) using Eq. 15 and were normalized to a value of 1 at 270 nm. (B) Wavelength dependence of slope factor. The slope factors from the fits to the results in Figs. 7 B and 8 are plotted as a function of wavelength on linear coordinates. The experimental points (●) are mean ± SD. Dashed lines show the range of the estimated slope factors for excitation wavelengths between 260 and 310 nm.

that at 300 nm by ~45% compared with the uncorrected values. No other corrections or adjustments were made to any of the spectra in Fig. 9 A aside from the normalization at 270 nm.

The channels' action spectrum (Fig. 9, ●) matched the calculated tryptophan action spectrum (solid line) quantitatively over most of its extent (260–310 nm). This close agreement indicates that the main photochemical effects on the channels were initiated by tryptophan absorption. The tyrosine spectrum declined more steeply than the channels' action spectrum, particularly on the long-wavelength side of the peak, while the spectra of phenylalanine, cystine, and cysteine targets (not shown) bore little resemblance to the action spectrum and are omitted for clarity (see Fig. 3).

The channels' UV sensitivity was 4.5× larger at 320 nm and 7× larger at 330 nm than expected for absorption by tryptophan. At 250 nm, the sensitivity was 1.3× larger than expected for tryptophan absorption. These discrepancies may result from wavelength-dependent variations in the nature of the photoproducts or their quantum yield of formation. Possible sources of these variations are considered in the discussion.

The slope factors (n^* in Eq. 28) for the UV dose–response relations clustered between 1.12 and 1.60 (indicated by the dashed lines in Fig. 9 B) for excitation wavelengths between 260 and 310 nm. The wavelength invariance of the slope over this region of the spectrum suggests that wavelength affects only the probability of absorption, and not the efficiency or nature of the subsequent photochemistry. The UV dose–response relation was significantly steeper for excitation at 250 nm ($n^* = 1.92$), and significantly shallower for 320 or 330 nm UV ($n^* = 0.69$ and 0.87, respectively). Interestingly, the channel action spectrum and the tryptophan spectrum deviated at these same wavelengths (Fig. 9 A). The simplest explanation for these results is that UV irradiation of the channels generated at least two different photoproducts with distinct effects on channel function. The slopes of the UV dose–response relations at 250, 260–310, and 320–330 nm would likely vary if the photoproducts were formed in different relative proportions after irradiation at those wavelengths. However, the slopes of the curves are not expected to vary with wavelength if UV produced a single photoproduct with a wavelength-dependent quantum yield, or generated multiple photoproducts in the same relative proportions at different wavelengths.

Effect of Environment on Tryptophan Absorption

Previous studies indicated that inserting tryptophan into a protein matrix shifts λ_{max}, the wavelength of maximal absorbance, by about +4 nm at most, and has negligible effect on the spectral lineshape (McLaren and Shugar, 1964; Matthews et al., 1973). The relative insensitivity of λ_{max} to environment is in marked contrast to the extremely large protein-induced shifts (up to −45 nm) in the wavelength of maximal tryptophan fluorescence (Lakowicz, 1983).

What is the environment of the target tryptophans in the channel? We approached this question by measuring the spectrum of the tryptophan derivative *N*-acetyl l-tryptophan amide (NATrpA) in a variety of organic solvents and comparing it with the action spectrum of channel modification. NATrpA is a popular model for protein tryptophans because of the similarity of its acetyl and amide linkages to the peptide linkages of

tryptophans in proteins (Lakowicz, 1983). Changing the solvent from aqueous buffer to organic solvent had the same effect as inserting tryptophan into a protein (Fig. 10 A). The polar solvents methyl alcohol and acetonitrile shifted λ_{max} by only +1.0 and +1.3 nm, respectively, relative to the value for tryptophan in aqueous buffer. Ethyl alcohol, which contains one more nonpolar methylene group than methyl alcohol, shifted the spectrum by +2.6 nm. Dimethylformamide and dimethylsulfoxide, which contain many of the functional groups present in nonpolar amino acids, shifted the spectra by +3.4 and +4.1 nm, respectively. These values are comparable with the largest shifts observed for buried tryptophans in proteins. The lineshape of the spectra were not altered appreciably by the solvent, as evidenced by their unchanged bandwidth and the preservation of distinct "shoulders" on the short and long wavelength sides of the peak in all solvents tested.

Because the tryptophan spectra are relatively flat near the peak at 280 nm, but very steep at 300 nm, shifts of only a few nanometers in λ_{max} may alter the ratio of absorption at these two wavelengths by a large factor. The 280/300-nm absorption ratio varied between values of 15.7 for tryptophan in buffer and 4.3 for NATrpA in DMSO, with intermediate values in the other solvents (Fig. 10 B). The 280/300-nm UV sensitivity ratio of CNG channels (17.1 ± 2.0) is consistent with the absorption of tryptophan in aqueous solution, but not with the absorption by NATrpA in any of the organic solvents tested, suggesting that the target tryptophans in the channels occupy a water-like chemical environment.

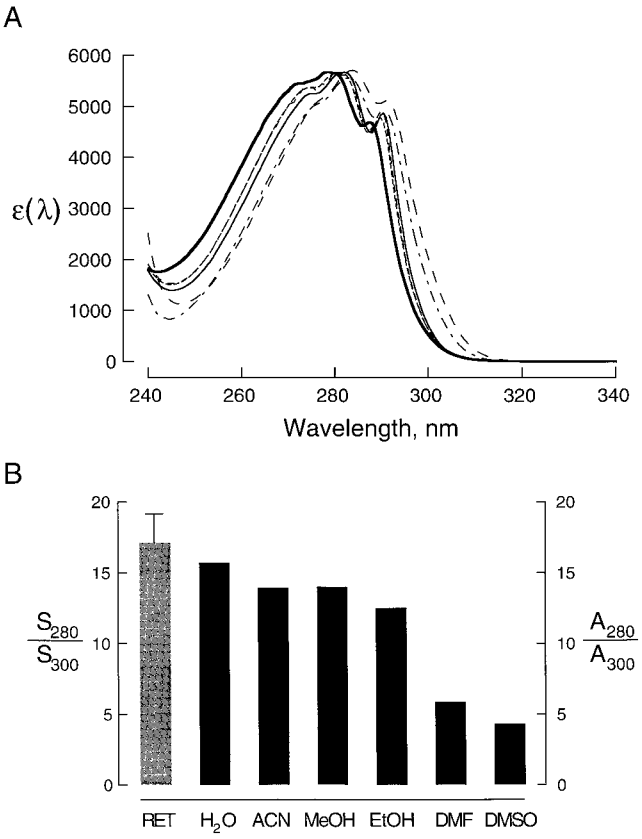

Figure 10. Environmental effects on tryptophan absorption. (A) Absorption spectra of tryptophan (trp) in aqueous buffer, and the tryptophan derivative NATrpA in various organic solvents. The compounds/solvents, symbols, solvent abbreviations, wavelengths of maximal absorption, and spectral widths (FWHM in nanometers) were: trp/water (solid bold line, H_2O, 279.7 nm, 37.7); NATrpA/acetonitrile (thin dashed line, ACN, 281.0 nm, 35.9); NATrpA/methanol (bold dashed line, MeOH, 280.7 nm, 35.7); NATrpA/ethanol (thin solid line, EtOH, 282.3 nm, 35.4); NATrpA/*N*,*N* dimethylformamide (dot-and-dashed line, DMF, 283.1 nm, 35.0); and NATrpA/dimethylsulfoxide (long dashed line, DMSO, 283.8 nm, 35.1). Extinction coefficients ($M^{-1} \cdot cm^{-1}$) are plotted as a function of wavelength on linear coordinates. The spectra in organic solvents are scaled to the same maximal extinction coefficient as that of tryptophan in buffer to facilitate comparison. (B) Comparison of tryptophan absorption in different solvents to CNG channel action spectrum. The right-hand ordinate shows the ratio of the tryptophan absorption probability at 280 and 300 nm, A_{280}/A_{300}. The absorption ratios were computed from the spectra in A using Eq. 15. The ratios were: Trp/H_2O, 15.7; NATrpA/ACN, 13.9; NATrpA/MeOH, 14.01; NATrpA/EtOH, 12.5; NATrpA/DMF, 5.8; and NATrpA/DMSO, 4.3. The UV sensitivity ratio of RET channels at these same wavelengths (S_{280}/S_{300}, left-hand ordinate) was 17.1 ± 2.0 (Figs. 8 and 9).

UV Photolysis of Tryptophan in Solution

Do tryptophan targets in CNG channels undergo the same photochemical reactions as free tryptophan in solution? The photochemistry of tryptophan in a protein may differ from that in solution because the photoexcited residues may react with surrounding protein residues (Creed, 1984a). The quantum yields and the distribution of photoproducts may even vary for different tryptophans in the same protein (Tallmadge and Borkman, 1990; McKim and Hinton, 1993). Since previous studies of tryptophan photochemistry were performed with different wavelengths and solvents than used here, we measured the photochemical conversion of tryptophan to its photoproducts using the same light source and solutions employed in our channel modification experiments.

We monitored the photolysis of tryptophan in aqueous solution spectrophotometrically. Irradiation at 280 nm converted the initial tryptophan absorption peak centered at 280 nm into a broad, diffuse band (Fig. 11 A). The absorbance changes indicate that the tryptophan photoproducts absorb more strongly than tryptophan from 230–270 nm and at wavelengths longer than 290 nm, but less strongly than tryptophan from 270 to 290 nm. The nature of the spectral changes in Fig. 11 A are consistent with the formation of the photoproducts in Fig. 1: kynurenine absorbs UV maximally at 230, 257, and 360 nm, while *N*-formyl kynurenine ab-

sorbs strongly at 235 and 318 nm (Walrant and Santus, 1974). Serine and aspartic acid do not absorb appreciably at wavelengths longer than 240 nm.

Assuming that the components in the solution absorb light independently, the sample absorbance after a UV dose D is the sum of the absorbances of the solutes (Calvert and Pitts, 1966):

$$A(D) = \sum_i \varepsilon_i b c_i(D). \quad (44)$$

In Eq. 44, ϵ_i and $c_i(D)$ are the extinction coefficient and molar concentration of the ith component, respectively, and b is the sample pathlength. For the scheme in Fig. 1, the sample absorbance is expected to vary with dose according to

$$\frac{\Delta A(D)}{\Delta A(\infty)} = 1 - \exp\left(-\sigma \sum_i \phi_i D\right), \quad (45)$$

where $\Delta A(D)$ is the absorbance change as a function of dose, $\Delta A(\infty)$ is the maximal absorbance change, σ is the absorption cross section of tryptophan at the exciting wavelength, and ϕ_i is the photochemical quantum yield for forming the ith photoproduct. Photochemical modification of tryptophan by 280 nm UV was monitored at 280 and 310 nm (Fig. 11 B). The absorbance change at each probe wavelength depended exponentially on UV dose, as shown by the fits of Eq. 45 (solid curves) to the results. The apparent quantum yield for the absorbance change at 310 nm (0.026 ± 0.002) was smaller than that at 280 nm (0.055 ± 0.005). A likely explanation for the difference in quantum yields at the two probe wavelengths is that the absorbance change at 280 nm reflects mainly the disappearance of tryptophan, which depends on the quantum yield for forming all primary photoproducts, while the absorbance change at 310 nm reflects both the formation of *N*-formyl kynurenine and its conversion to secondary photoproducts (see discussion).

The UV dose that caused a half-maximal change in tryptophan absorbance at 280 nm (5.8×10^9 photons · μm^{-2}, Fig. 11) was remarkably similar to the $D_{1/2}$ value for current reduction in CNG channels activated by saturating cGMP at the same wavelength (4.6×10^9 photons · μm^{-2}, Fig. 8). The similarity of these values suggests that UV modifies tryptophan in solution and tryptophan targets in the channels with nearly equal efficiencies.

UV Sensitivity of Tryptophan Mutants

Which tryptophans in CNG channels are the UV targets? Fig. 12 A is a schematic diagram showing the location of the 10 tryptophan residues in a CNG channel subunit. Many of the tryptophans are located in channel domains that are involved in activation gating, such as W9, W166, and W178 in the N-S2 domain, W353 in the channel pore, and W435 and W440 in the C-linker.

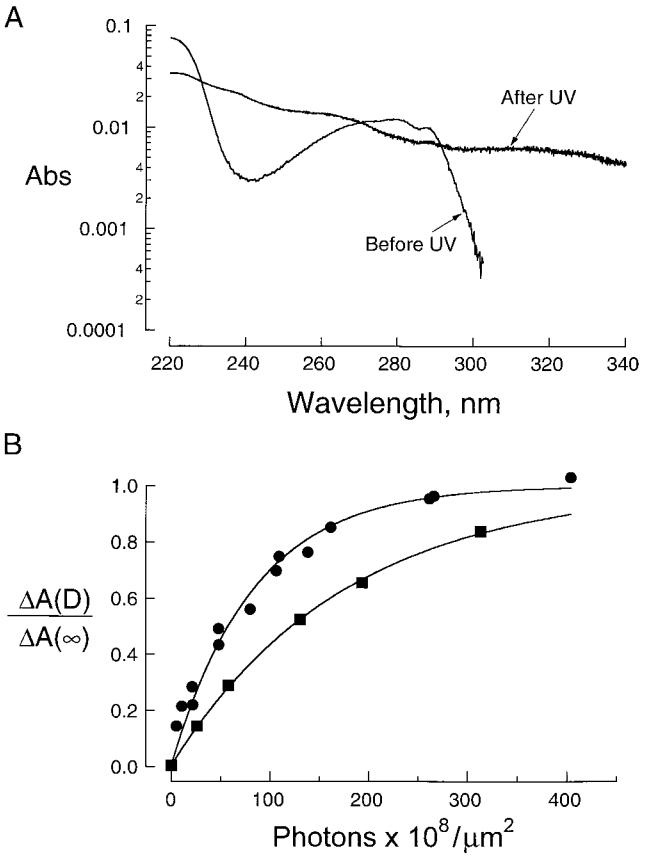

Figure 11. UV modification of free tryptophan in aqueous solution. (A) Effect of UV irradiation on the absorption spectrum of tryptophan. Absorption spectra of 25 μM tryptophan in standard sodium solution (see materials and methods), pH 7.6, before UV and after exposure to 3.13×10^{10} photons · μm^{-2} at 280 nm. (B) Dose dependence of UV modification of free tryptophan. Photochemical modification of tryptophan by 280 nm UV was followed by monitoring the absorbance changes at 280 nm (●) and 310 nm (■). The absorbance change at each wavelength [ΔA(D)] normalized to the maximal absorbance change at the same wavelength [ΔA(∞)] is plotted as a function of the photon dose. Smooth curves are fits to the absorbance changes using Eq. 45. Half-maximal UV doses ($D_{1/2}$) and total photochemical quantum yields ($\Sigma\phi_i$, see Eq. 45) were 57.8×10^8 photons · μm^{-2} and 0.055 ± 0.005, respectively, at 280 nm and 122.8×10^8 photons · μm^{-2} and 0.026 ± 0.001, respectively, at 310 nm.

We attempted to locate the UV targets by examining the UV sensitivity of channels in which tryptophans were replaced by other amino acids. If the mutations have no effect on the channels other than to alter their tryptophan content, then the UV sensitivity of some of the mutant channels should be reduced or possibly abolished. Cyclic GMP-activated currents were not detected for a tryptophan-less channel, or for any of a number of mutant channels that lack more than one of the native tryptophans in each subunit. In contrast, all of the 10 possible mutants lacking a single tryptophan per subunit yielded functional channels. Exposure to 280 nm UV reduced the current through each of these

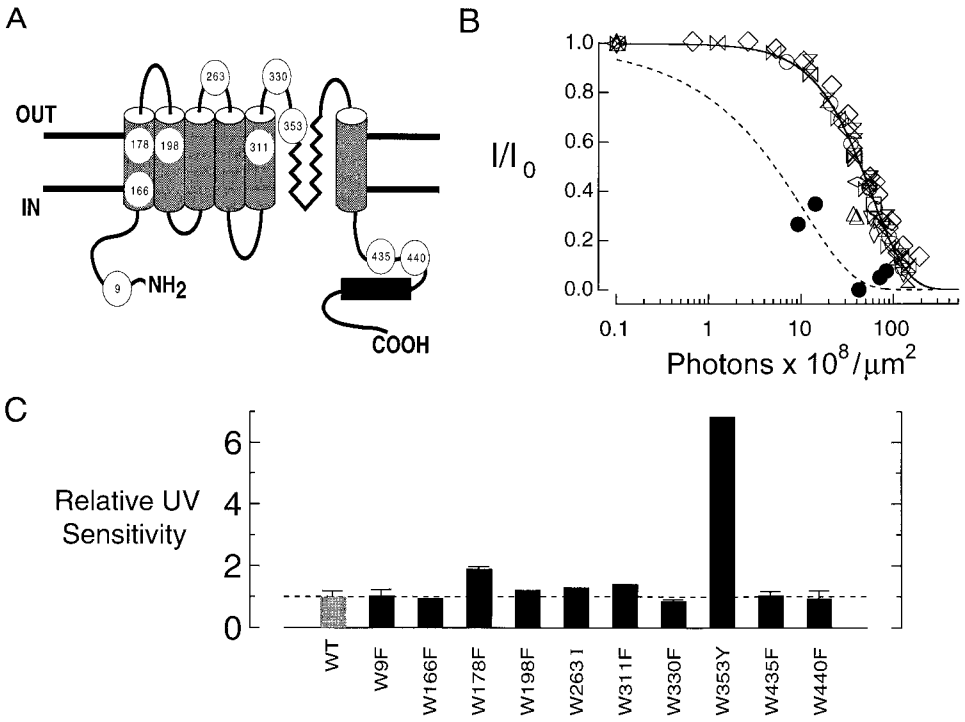

Figure 12. UV sensitivity of CNG channel tryptophan mutants. (A) Schematic diagram of RET channel α subunit indicating the positions and presumed locations of the 10 tryptophan residues in each subunit of the bovine retinal cGMP-gated channel. (B) UV dose–response relations of RET channel tryptophan point mutants. Each type of symbol represents collected results for one mutant. Mutations, $D_{1/2}$ values in photons $\cdot 10^8 \cdot \mu m^{-2}$, and the corresponding symbols are: W9F, 43.9 (○); W166F, 47.7 (□); W178F, 24.1 (△); W198F, 37.4 (▽); W263I, 35.1 (wide diamond); W311F, 32.6 (tall diamond); W330F, 52.8 (◇); W353Y, 6.7 (●); W435F, 43.3 (▷◁); and W440Y, 47.8 (hourglass). The dashed curve is a fit to the results for W353Y channels using Eq. 28; the solid curve is a fit of this model to the collected results for all other mutants. Channels were irradiated in the absence of ligand at 280 nm. (C) Comparison of UV sensitivities of wild-type and tryptophan mutant channels. UV sensitivities, relative to the value for wild-type (WT) RET channels, are shown on the ordinate for each tryptophan point mutant.

mutants to a small fraction of its initial value (Fig. 12 B), indicating that the channels must contain more than one target tryptophan residue per subunit.

The UV sensitivities of 9 of the 10 tryptophan mutants were similar to that of wild-type channels (Fig. 12 C). In addition, the slopes of their UV dose–response relations (average $n^* = 1.33 \pm 0.04$) were similar to that of wild-type channels ($n^* = 1.39 \pm 0.05$), suggesting that the mutations did not alter the mechanism of the current reduction by UV.

One of the mutant channels was unusual. W353Y channels, in which tyrosine replaces a highly conserved tryptophan residue in the channel pore, were approximately seven times more UV sensitive than wild-type channels. This result was unexpected since W353Y channels contain fewer tryptophan residues than wild-type channels. Possible mechanisms for the anomalous behavior of W353Y channels are considered below and in the accompanying paper (Middendorf and Aldrich, 2000). The UV dose–response relation of W353Y channels may also be shallower than that of wild-type channels; however, due to the limited number of experimental points, the apparent difference in slope was not statistically significant.

Modeling of UV Dose–Response Relation

Does UV reduce CNG channel currents mainly by lowering the channels' open probability or by decreasing their unitary conductance? The UV-activated conductance (see above) made direct single channel measurements before and after UV impractical. Therefore, we adopted the alternative approach of analyzing the 280-nm UV dose–response relations of wild-type and W353Y mutant channels using the three physical models for UV modification described in the theory section (above). For each model, the quantum yield for target modification was estimated for various target numbers, using the fitting parameter $\sigma \cdot \phi$ (see Eqs. 28, 33, and 40), and an absorption cross section of 2.17×10^{-17} cm^2 for free tryptophan in aqueous solution at 280 nm (Fig. 3). The total number of UV targets per channel was assumed to be $4n$ (where n is the number of targets per subunit), consistent with the tetrameric composition of the channels (Liu et al., 1996; Morrill and MacKinnon, 1999). For simplicity, each model assumes that the UV targets are independent and identical.

The all-or-none model assumes that UV has no effect on channel function until a critical number of target residues (n^*) are modified, which renders the channel nonconducting. The model does not distinguish between UV effects on the channel's unitary conductance and open probability (see Eq. 26). Fits of this model (Eq. 28) to the UV dose–response relation of wild-type channels for various values of n^* are shown in Fig. 13 A. The simulated curves were very sensitive to the values of n^* and the quantum yield ϕ. Varying ϕ shifted the curves horizontally without altering their shape, while changing n^* affected both the position of the curves on

the abscissa and their slope. The fits were not sensitive to the total number of targets, although increasing this parameter had the effect of increasing the total effective absorption cross section of the targets, which caused a proportional decrease in the estimated quantum yield (Eq. 28). For all possible values of n ($1 \leq n \leq 10$), the relations for wild-type channels were fit equally well using critical target numbers of 1 or 2. The curves for $n^* = 1$ were slightly shallower than the observed relations, while the curves for $n^* = 2$ were slightly steeper than the experimental points. The simulated relations for $n^* > 2$ were much steeper than the experimental points, establishing an upper limit of 2 for the critical target number. The quantum yields obtained from the fits depended on both n and n^*, and varied from 0.0018 for $n = 10$, $n^* = 1$ to 0.048 for $n = 1$, $n^* = 2$.

It is reasonable to assume that the "effective" quantum yield for modifying targets in W353Y mutant channels is less than or equal to that for wild-type channels, since the mutant channels contain one less tryptophan residue. (We define effective quantum yield as the quantum yield for modifying one target multiplied by the number of targets.) If the other model parameters (i.e., n and n^*) were kept the same as for wild-type channels, decreasing the value of ϕ had the effect of shifting the simulated curves to the right along the abscissa. This shift is opposite the observed leftward shift of the UV dose–response relation for W353Y channels compared with wild-type channels (Fig. 12 B). The only way to shift the relation for W353Y channels to the left of the relation for wild-type channels was by decreasing n^*. Since $n^* \leq 2$ for wild type channels (see above), this condition could only be satisfied if $n^* = 1$ for W353Y channels. Simulated UV dose–response relations were generated for all possible values of n for W353Y channels, assuming $n^* = 1$ and using the quantum yields obtained for wild-type channels with $n^* = 2$ and the same value of n. The simulated curves for W353Y were well to the right of the experimental points for all values of n. This failure of the all-or-none model to fit the UV dose–response relations of the wild-type and mutant channels simultaneously suggests that UV reduced the channel currents in a graded fashion.

The proportional conductance model assumes that each UV target modification decreases the channels' unitary current by an equivalent amount. This model might apply if the channels' unitary conductance decreased stepwise as targets in each subunit were modified. In fact, Liu et al. (1996) showed that the unitary conductances of heteromultimeric channels composed of retinal and olfactory channel subunits are intermediate to the single channel conductances of the parent channels, and scale in proportion to the number of large-conductance subunits.

The fits to the UV dose–response relation of wild-

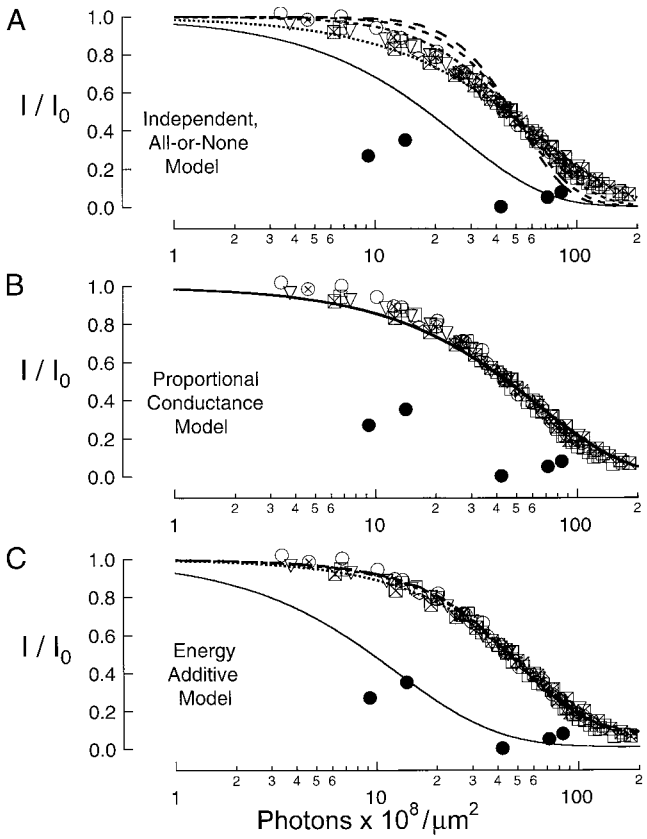

Figure 13. Modeling of UV dose–response relation. (A) Independent, all-or-none model. UV dose–response relation of CNG channels irradiated with 280 nm UV. Open symbols represent results for wild-type RET channels; solid symbols are for W353Y mutant channels. Channels were irradiated in the absence of ligand. Smooth curves are fits of the independent, all-or-none model (Eq. 28) to the collected results for each type of channel. The critical target number (n^*) was set to one (narrow dotted line), two (dotted line), three (long dotted line), or four (dashed line) for wild-type channels. Also shown is the best fit (solid line) to the UV dose–response relation of RET W353Y channels for $n = 2$ and $n^* = 1$. A total of two targets per channel subunit was assumed in the fits; however, this parameter had little effect on the quality of the fits, which was determined mainly by the slope factor n^*. (B) Proportional conductance model. Smooth curves are fits of the proportional conductance model (Eq. 33) to the same results as shown in A. The simulated curves were independent of the total target number n. The best fit to the results for wild-type channels (solid line) was obtained for $\phi = 0.072$. Simulated curve for W353Y was identical to the curve for wild-type channels if the same quantum yield was assumed. (C) Energy additive model. Smooth curves are fits of the energy additive model (Eq. 40) to the same results as shown in A assuming one to four targets per subunit for wild-type channels and using a free energy difference $\Delta G^0(0)$ of -3.0 *RT*. Also shown is a fit to UV dose–response relation of W353Y channels (solid line) with the quantum yield for target modification fixed to the same value as that of wild-type channels and assuming three targets per subunit and $\Delta G^0(0) = +4.0$ *RT*. Fitting parameters for all three models are summarized in Table I.

type channels were identical for all values of n (see Eq. 33) and were somewhat shallower than the results (Fig. 13 B). The proportional conductance model was ruled out because it could not reproduce the leftward-shift of the UV dose–response relation of W353Y channels relative to that of wild-type channels without violating the constraint that the photochemical quantum yield for W353Y channels must be less than or equal to that for wild-type channels (see above).

The energy additive model assumes that UV lowers the channels' open probability by stabilizing the closed channel relative to the open channel. For simplicity, it was assumed that each target modification exerts an equal and additive effect (represented by the parameter $\Delta\Delta G^0(1)$, see Eq. 40) on the free energy difference between the channels' open and closed states. The model fit the UV dose–response relation of wild-type channels well for all possible target numbers ($1 \leq n \leq 10$, Fig. 13 C). The free energy "cost" of modifying a single target, $\Delta\Delta G^0(1)$, varied inversely with the value of n, and the total energetic cost of modifying all of the UV targets, $4n \cdot \Delta\Delta G^0(1)$, remained roughly constant for different values of n. In contrast to the all-or-none and proportional conductance models, the energy additive model also reproduced the observed leftward shift of the UV dose–response relation of W353Y channels. The relations for wild-type and W353Y channels could be fit simultaneously using the same values of n, ϕ, and $\Delta\Delta G^0(1)$ for both channels, but only if $\Delta G^0(0)$ was much more positive for W353Y channels. This finding suggests that the mutation lowered the channels' open probability substantially. Other observations are consistent with this idea. Cyclic GMP-dependent currents were not observed for this mutant initially, but were rescued by the application of low cytoplasmic concentrations of Ni^{+2} ions to the patches, which increases the open probability of RET channels (Gordon and Zagotta, 1995a). This observation suggests that the UV sensitivity of W353Y channels is anomalously high because the tryptophan-to-tyrosine substitution "cripples" the channels (in an energetic sense), leaving them more susceptible to UV. The companion paper (Middendorf and Aldrich, 2000) provides additional evidence in favor of this hypothesis. We conclude that UV modification involves mainly a change in channel open probability rather than a change in single channel conductance.

The fitting parameters for all three models are compiled in Table I.

UV Effect on Ion Selectivity

We favor the idea that the main effect of UV is on the open probability of CNG channels, but cannot rule out some effect on the channels' unitary conductance. We tested this model-dependent conclusion in another way by measuring the ion selectivity of modified channels. Although CNG channels do not discriminate between monovalent cations as finely as related channels such as *Shaker* potassium channels, they do exhibit ion selectivity. For example, they are about nine times more permeable to ammonium ions than to cesium ions (Kaupp et al., 1989). If UV greatly reduced the unitary conductance of CNG channels, it would likely alter other pore properties of the channels as well, such as their ion selectivity. We investigated possible UV effects on the pore of CNG channels by measuring the channels' permeability to several different monovalent cations before and after irradiation (Hille, 1992). In all experiments, 130 mM NaCl was present in the pipet (extracellular) solution, while the bath (intracellular) solution contained 130 mM of either LiCl, NaCl, KCl, NH_4Cl, RbCl, or CsCl. Currents elicited by voltage ramps between −50 and +50 mV are shown in Fig. 14. A UV dose that reduced the current in 130 mM symmetrical NaCl to one-third its initial amplitude at +50 mV did

TABLE I

Modeling of Wild-Type UV Dose–Response Relation

Model	Parameters			
	UV targets			
	Total No.	Critical No.	Quantum yield	$\Delta\Delta G^0(1)$
	4n	*n**		
Independent, all-or-none				
	4	1	0.0178 ± 0.0002	
	4	2	0.0479 ± 0.0005	
	4	3	0.093 ± 0.002	
	4	4	0.180 ± 0.003	
	8	1	0.0089 ± 0.0001	
	8	2	0.0221 ± 0.0002	
	8	3	0.0375 ± 0.0006	
	8	4	0.056 ± 0.001	
Proportional conductance				
	4		0.0715 ± 0.0008	
	8		0.0715 ± 0.0008	
	12		0.0715 ± 0.0008	
	16		0.0715 ± 0.0008	
Energy Additive				
	4		0.060 ± 0.005	1.76 ± 0.12
	8		0.074 ± 0.002	0.75 ± 0.02
	12		0.079 ± 0.002	0.48 ± 0.01
	16		0.082 ± 0.002	0.35 ± 0.01

Summary of UV parameters obtained from modeling of UV dose–response relation for wild-type RET channels activated by saturating (1 mM) cGMP. Results were fit using the all-or-none model (Eq. 28), the proportional conductance model (Eq. 33), and the energy additive model (Eq. 40). Parameter values are mean ± SD. For the energy additive model, an initial standard free energy difference [$\Delta G^0(0)$] of −3.0 *RT* was used, which corresponds to an open probability of 0.95. The estimated values for $\Delta\Delta G^0(1)$, the free energy cost of target modification, are also given in *RT* units; *RT* = 0.58 kcal/mol.

not shift the reversal potential significantly for any of the cations tested. The permeability of each cation relative to that of Na^+ was computed from the corresponding reversal potential (V_{rev}) using the Goldman-Hodgkin-Katz equation:

$$\frac{P(X^+)}{P(Na^+)} = \exp\left(-\frac{zF\,V_{rev}}{RT}\right). \quad (46)$$

In Eq. 46, F is the Faraday constant and z is the charge on the ions (+1). The magnitude and rank order of the relative cation permeabilities were very similar before and after irradiation.

The relative effect of UV on the amplitudes of currents carried by the different monovalent cations provided a second measure of possible UV effects on permeation. The ratio of the outward current amplitudes before and after UV were computed for each ion after first correcting the current–voltage relations for the small changes in reversal potential after irradiation. The fractional reduction in current was similar for all ions tested (Fig. 15 B). The results in Figs. 14 and 15 thus provide no evidence for UV effects on ion permeation through CNG channels, consistent with the idea that the main effect of UV is on the channels' open probability.

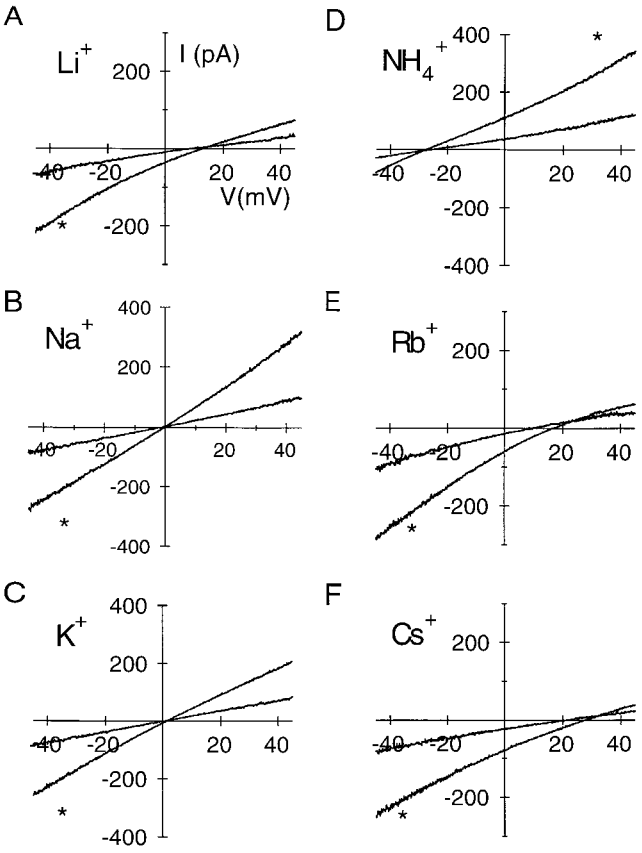

Figure 14. Effect of UV light on currents carried by different monovalent cations. (A–F) RET channel currents in the presence of 500 μM cGMP before UV (*) and after exposing patch to a dose of 5.07×10^9 photons · μm^{-2} from a high-intensity pulsed UV laser (λ = 266 nm). The pipet contained 130 mM NaCl for all experiments, and the bath solution contained 130 mM of LiCl (A); NaCl (B); KCl (C); NH_4Cl (D); RbCl (E); or CsCl (F). Reversal potentials (mV) before and after irradiation were: (A) 12.6 and 8.6; (B) 0 and 0; (C) 1.1 and −0.1; (D) −27.4 and −25.7; (E) 17.0 and 10.0; and (F) 28.4 and 22.3. The voltages were not corrected for junction potentials. The patch was irradiated in the presence of 100 μM cGMP. The voltage was ramped between −50 and + 50 mV in 600 ms. The laser intensity was 1.49×10^{16} photons · $\mu m^{-2} \cdot s^{-1}$.

DISCUSSION

Interpretation of Action Spectrum

The irreversible reduction of current through CNG channels by UV light involves two distinct steps. Membrane particles that we call "initiators" absorb the UV photons. The energy of the absorbed photons drives subsequent photochemical transformations of membrane particles that we refer to as "targets." It is the latter process that reduces the amplitude of the channel currents. Since UV reduced the currents to ≤5% of their pre-UV amplitude, it is likely that the targets are intrinsic to the CNG channels. We cannot rule out the alternate possibility that the targets are located in other membrane components that interact strongly with the channels.

The close agreement between the channels' action spectrum and the absorption spectrum of tryptophan in aqueous solution (Figs. 9 and 10) indicates that the main initiators of target modification are tryptophan residues occupying a water-like environment. Three distinct photochemical mechanisms might be triggered by absorption in tryptophan. Mechanism I (depicted in Fig. 1) assumes that the photochemical modifications that reduce the channel currents occur in the same tryptophan residues that initially absorb UV.

Mechanism II assumes that the initial light-absorbing tryptophans are not themselves modified by UV, but rather that these initiators sensitize the excitation of other amino acids (the target residues) by resonance energy transfer (Weber, 1960; Lakowicz, 1983). This type of mechanism has been proposed to explain the high UV sensitivity of acetylcholinesterase (Bishop et al., 1980). In proteins, tryptophan residues transfer energy almost exclusively to other tryptophans within ~20 Å (Weber, 1960; Lakowicz, 1983). The efficiency of the transfer depends on the overlap between the fluorescence emission spectrum of the sensitizer (initiator) tryptophan and the absorption spectrum of the acceptor (target) tryptophan (Turro, 1978). The fluorescence spectrum of solvent-exposed protein tryptophans, denoted E, is shifted to much longer wavelengths than that of buried tryptophans, denoted B (Lakowicz, 1983), but the absorption spectrum of tryp-

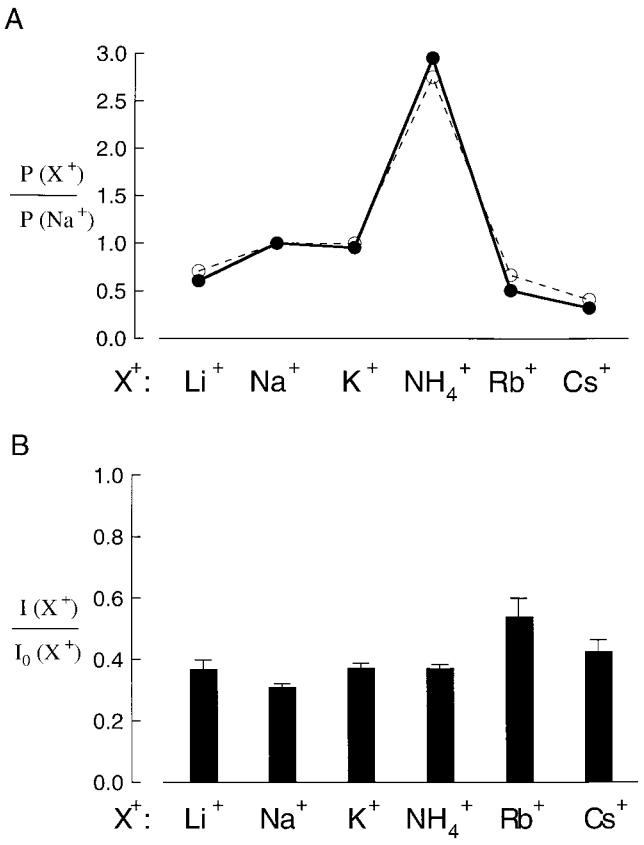

Figure 15. (A) Effect of UV light on relative monovalent cation permeabilities of RET channels. The permeability ratios of various monovalent cations ($X^+ = Li^+$, Na^+, K^+, NH_4^+, Rb^+, and Cs^+) relative to that of Na^+ are plotted before (●) and after (○) UV irradiation of the channels. Permeability ratios were calculated from the Goldman-Hodgkin-Katz equation (Eq. 46) using the reversal potentials obtained from the results in Fig. 14. (B) UV effect on RET channel currents carried by different monovalent cations. The ordinate shows the outward current amplitude after UV irradiation, I(*D*), divided by that before UV, I(0), for the results in Fig. 14.

tophan is much less sensitive to environment (Fig. 10). The spectral overlap factor is therefore very unfavorable for energy transfer from E → B or E → E. The solvent-exposed initiator tryptophans in CNG channels (Fig. 10) thus are unlikely to act as efficient photosensitizers of other tryptophans, ruling out energy transfer as an important mechanism for target modification in the channels.

Mechanism III proposes that the photo-excited initiator tryptophan residues react with nearby residues in the channel protein, and that the covalent modification of these neighboring amino acids (the target residues) reduces the channel current. The target residues need not be tryptophans. For example, in some proteins, photoexcited initiator tryptophans may undergo redox reactions with nearby disulfide targets (Vladimirov et al., 1970).

Although we cannot rule out Mechanism III, we note that the half-maximal doses for tryptophan photolysis in solution (Fig. 11 B) and channel current reduction (Fig. 8 A) by 280 nm UV are very similar. This similarity suggests that the photochemistry of the targets in the channels is like that of isolated tryptophans. Therefore, we favor the idea that UV absorption by channel tryptophans, and the subsequent photochemical modification of those same residues, causes the current reduction in CNG channels (Mechanism I).

As noted above, the CNG channel action spectrum and the tryptophan absorption spectrum differed at 250 and 320–330 nm (Fig. 9 A). There are several possible reasons for these discrepancies. RET channels contain a large number of residues other than tryptophan that absorb in the 250–330-nm range, including 30 tyrosines, 33 phenylalanines, and 7 cysteines per subunit. These other amino acids may contribute additional spectral components to the channels' action spectrum if they initiate photochemical reactions that alter the channel currents. We tested for such components by fitting the action spectrum to linear combinations of the absorption spectra of tryptophan and the other UV-absorbing amino acids. As shown in Fig. 16, adding together tryptophan and cystine absorption spectra in roughly equal proportions (based on the molar extinction coefficients of the two compounds, see Fig. 3) provided an excellent fit to the channel action spectrum over the entire range of wavelengths studied. The action spectrum is a weighted average that depends on: (a) the number of each type of initiator residue, (b) the absorption spectra of the individual initiators, (c) the relative nature and quantum yields of the photoproducts formed from modification of the target residues, and (d) the magnitude of the current loss associated with formation of each of these photoproducts. These complications prevent us from estimating the relative effects on channel function of modifying a single tryptophan target compared with a single cystine target. However, the fit to the action spectrum in Fig. 16 suggests that tryptophan photolysis dominates the UV effect at excitation wavelengths shorter than 315 nm, while cystine photolysis is the more important effect at longer wavelengths.

Experiments using the cross-linking reagent copper phenanthroline (CuPhe) indicate that disulfide formation between cysteines in the amino- and carboxy-terminal regions of CNG channels stabilize the channels' open state (Gordon et al., 1997). Those workers found that dithiothreitol (DTT) had no effect on the channel currents before CuPhe treatment, suggesting that expressed channels normally do not contain disulfide linkages. However, as with all chemical-modification experiments, the lack of effect may result from inaccessibility of the reagent to its intended target. Alternatively,

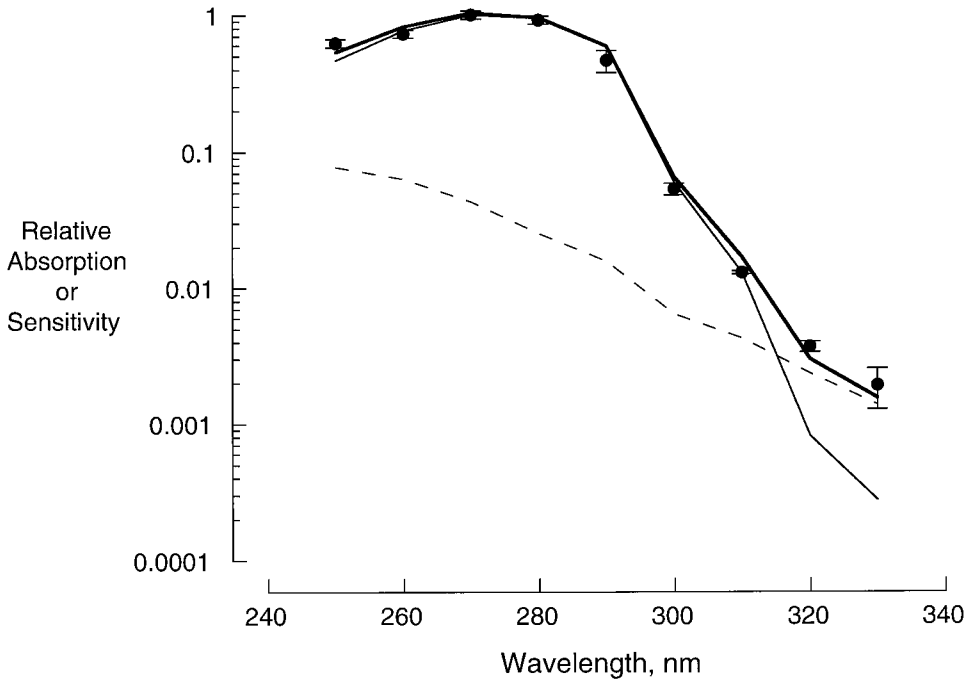

Figure 16. Contribution of cystine photolysis to UV effect on CNG channels. Symbols show the action spectrum of the UV effect on RET channels (mean ± SEM, ●, results from Fig. 9 A). Also shown is a fit to the action spectrum (bold line) using a linear combination of the filter-corrected absorption spectra (see materials and methods and Fig. 3) of tryptophan (thin line) and cystine (dashed line) in aqueous buffer. Relative contributions of the spectral components were 1.0 for tryptophan and 0.93 for cystine.

DTT and UV may have different effects on the channels because of possible differences in the products formed by each reagent (Creed, 1984c). If disulfides are present, our results suggest that their modification by UV reduces the channel current. We note that UV modification of cystine residues has been shown to photoinactivate other enzymes (Luse and McLaren, 1963; McLaren and Shugar, 1964).

Adding tyrosine or phenylalanine spectral components to the tryptophan absorption spectrum did not improve the fit to the channels' action spectrum, suggesting that these residues are not modified by UV, or that their photochemical modification does not alter channel function significantly.

A second mechanism may also contribute to the channels' anomalously high UV sensitivity (relative to tryptophan absorption) at wavelengths longer than 320 nm. The absorption cross section of the tryptophan photoproduct *N*-formyl kynurenine (NFK; Fig. 1) is so much larger than that of tryptophan at 320 nm ($\epsilon \approx$ 3,180 vs. 3 M^{-1} cm^{-1}, respectively, see Walrant and Santus, 1974, and Fig. 3) that the absorption probability of the two compounds at this wavelength are equal after conversion of only 0.1% of the tryptophan to NFK. Absorption of 320 nm UV by NFK sensitizes the formation of the reactive oxygen species singlet oxygen, which has been shown to photo-oxidize tryptophan (Walrant and Santus, 1974). We find that exposing CNG channels to singlet oxygen formed by irradiation of triplet photosensitizer dyes reduces the currents in a manner similar to UV light (our unpublished observations). It is likely that singlet oxygen formed by irradiation of the primary tryptophan photoproduct NFK at long wavelengths may contribute to the UV effect on CNG channel currents. The photoproducts formed by direct UV photolysis of tryptophan compared with its photo-oxidation by singlet oxygen are almost certainly different, and may contribute to the difference in the slopes of the UV dose–response relations for short (260–310 nm) versus long (≥320 nm) excitation wavelengths (Fig. 9 B).

Target Number

How many tryptophan targets (denoted n_{eff}) must be modified to reduce the channel current by 50% or more? The UV dose–response relations of wild-type and W353Y mutant channels were inconsistent with an all-or-none model for the UV effect (Fig. 13 A), indicating that the current reduction required modification of more than one target. Although the relations were consistent with the energy-additive model, the analysis did not provide an upper limit for n_{eff}.

Our results also did not provide an exact estimate for the total number of tryptophan targets (denoted n_{tot}) in CNG channels. However, two lines of evidence suggest that only a subset of the 10 tryptophans per channel subunit are targets. First, the channels' action spectrum is similar to the spectrum of free tryptophan in solution, but inconsistent with the spectrum of fully or partially buried tryptophans (Fig. 10). Many of the channel tryptophans are in transmembrane segments of the channel (Fig. 12 A), where they are probably not exposed fully to solvent. Second, the UV dose required

to photolyze tryptophan in aqueous solution (Fig. 11) was very similar to the dose that reduced the currents through CNG channels (Fig. 8). The simplest explanation for this similarity is that the channels contain a small number of targets, and that their photochemical quantum yields are similar to the quantum yield for free tryptophan in solution. Since all 10 tryptophan point mutants remained sensitive to UV, the channels must contain more than one target per subunit. This observation is consistent with the conclusion (see above) that $n_{eff} > 1$, since $n_{tot} \geq n_{eff}$.

We were unable to locate the tryptophan targets within the channels' amino acid sequence, since all mutant channels that replaced individual tryptophans by other amino acids remained sensitive to UV. Since the channels contain more than one target residue per subunit (see above), it may be necessary to remove several tryptophans by mutagenesis to identify the UV targets. Results in the following paper (Middendorf and Aldrich, 2000) suggest that the apparent lack of expression of some of the mutant RET channels may actually be due to a very low open probability of the channels. The mutant channels may express better in the olfactory CNG channel background due to its more favorable gating properties (Goulding et al., 1994; Gordon and Zagotta, 1995b; Varnum and Zagotta, 1997).

Our results provide no information on the total or effective number of cystine targets in the channels.

Mechanism of Current Reduction by UV

Our analysis of the UV dose–response relations of wild-type and W353Y mutant RET channels (Fig. 13) suggests that UV reduces CNG channel currents primarily by lowering the channels' open probability rather than by decreasing their unitary conductance. This notion is supported by the lack of a UV effect on the channels' ion selectivity (Figs. 14 and 15). It is unlikely that changes in the channels' unitary conductance sufficient to produce the large current reduction by UV ($\geq$95%) could have occurred without significant changes in the structure of the channel pore. However, the channels' ion selectivity was essentially unchanged by UV (Fig. 15 A). It might be argued that UV effects on the channel pore were missed in those experiments because the current after UV was carried exclusively by unmodified channels. However, this idea implies an all-or-none mechanism for the UV effect, which was ruled out previously (Fig. 13 A). The following paper (Middendorf and Aldrich, 2000) provides additional evidence that the major effect of UV is on the channels' open probability rather than their unitary conductance.

We attempted to assess directly the magnitude of the UV effects on the channels' open probability and unitary conductance using single-channel methods. This approach was unsuccessful, however, because the currents through patches containing single CNG channels were overwhelmed by currents through UV-activated conductance sites (results not shown).

State Dependence of UV Effect

The ability of many reagents to block or chemically modify CNG channels depends on the channels' conformational state. For example, the pore blocker tetracaine binds much more tightly to closed than to open channels (Fodor et al., 1997a), while the sulfhydryl-modifying reagent *N*-ethyl maleimide and the disulfide-inducing reagent copper phenanthroline reacts more rapidly with open than with closed channels (Brown et al., 1998; Gordon et al., 1997). It is likely that the reactions are state-dependent because the physical access of the reagent to its site of action, or the electrostatic environment of that site, are different in the open and closed channel conformations. The state dependence of disulfide formation (Gordon et al., 1997) may also result from a difference in the relative proximity of the two component cysteine residues in open and closed channels.

In contrast to the results for blockers and chemical modifying agents, we found that UV reduced CNG channel currents with equal effectiveness when the channels were exposed to half-saturating cGMP or no cGMP (Figs. 7, A and B). A significant difference between the chemical and photochemical modification experiments is that the channels' conformation does not affect the "access" of photons to their targets appreciably: the absorption cross section of tryptophan is relatively insensitive to its environment (McLaren and Shugar, 1964), and the channel protein has insufficient optical density to "shield" the targets from UV. The similarity of the UV sensitivities of open and closed CNG channels suggests that either the functionally important photochemical modifications involve intramolecular rearrangements of tryptophan targets, or else that tryptophan initiators react with other protein residues whose proximity is not affected by channel activation.

A more subtle form of state dependence that we did not investigate is the possibility that the channels' action spectrum may be sensitive to the conformational state of the channels during irradiation.

Relation to Previous Work

Before the advent of modern molecular biological techniques, UV light was a preferred method for altering the sidechains of protein amino acids (McLaren and Shugar, 1964; Vladimirov et al., 1970; Grossweiner, 1976). UV modification of amino acids generally disrupts protein function. Ion channels are not immune to these deleterious effects: UV reduces the currents through voltage-activated sodium channels in nerve (Audiat et al., 1931; Booth et al., 1950; Lieberman,

1970; Fox and Stampfli, 1971; Oxford and Pooler, 1975) and muscle (Stühmer and Almers, 1982), and gramicidin A channels in planar lipid bilayers (Busath and Waldbillig, 1983; Kunz et al., 1995). We find that UV alters currents through cyclic nucleotide–gated channels from bovine retina (Figs. 6 and 8) and rat olfactory epithelium (Middendorf and Aldrich, 2000), and reported similar effects on voltage-activated *Shaker* K^+ channels previously (Middendorf et al., 1995).

The UV sensitivity of gramicidin channels is conferred by their tryptophan residues (Jones et al., 1986; Busath and Hayon, 1988; Strassle et al., 1989), while the UV effects on voltage-activated sodium channels are mediated by their tryptophan and/or tyrosine residues (Fox and Stampfli, 1971; Oxford and Pooler, 1975). The action spectra of CNG channels (Fig. 9) and *Shaker* channels (Middendorf et al., 1995) indicate that UV modification of tryptophan residues inhibits the currents through these channels as well. Taken together, these results suggest that at least some tryptophan residues are important to channel function. This conclusion is not surprising, given tryptophan's unique properties. Tryptophan has the lowest mutability of the 20 amino acids normally found in proteins (Creighton, 1993), and its indole sidechain has the largest volume (Richards, 1974; Chothia, 1975) and surface area (Miller et al., 1987) of any amino acid. The strong, favorable interactions of tryptophan with both water (Radzicka and Wolfenden, 1988) and lipid (Nozaki and Tanford, 1971; Radzicka and Wolfenden, 1988) are also unusual.

The authors thank Cynthia Adams and Christine Warren for experimental assistance in the early stages of this work, Steven Boxer for the generous loan of the Nd^{+3}:YAG laser, Laura Mazzola for critical reading of the manuscript, Steve Baylor, Dan Cox, and Alan Miller for helpful discussions, and Robert Schneeveis for excellent technical assistance.

This work was supported by grants from the National Institutes of Health (NS23294), the National Eye Institute (EY01543), and the McKnight Foundation. Richard W. Aldrich is an investigator with the Howard Hughes Medical Institute.

Submitted: 27 March 2000
Revised: 1 June 2000
Accepted: 5 June 2000

REFERENCES

Akabas, M.H., D.A. Stauffer, M. Xu, and A. Karlin. 1992. Acetylcholine receptor channel structure probed in cysteine-substitution mutants. *Science.* 258:307–310.

Altenhofen, W., J. Ludwig, E. Eismann, W. Kraus, W. Bönigk, and U.B. Kaupp. 1991. Control of ligand specificity in cyclic nucleotide–gated channels from rod photoreceptors and olfactory epithelium. *Proc. Natl. Acad. Sci. USA.* 88:9868–9872.

Audiat, J., D. Auger, and A. Fessard. 1931. Etude des courants d'action du nerf soumis au rayonnement ultra-violet. *Compt. Rend. Soc. Biol.* 107:1218–1221.

Augenstine, L.G., and C.A. Ghiron. 1961. The inactivation of trypsin by ultraviolet light. I. The correlation of inactivation with the disruption of constituent cystine. *Proc. Natl. Acad. Sci. USA.* 47:1530–1547.

Becchetti, A., K. Gamel, and V. Torre. 1999. Cyclic nucleotide-gated channels. Pore topology studied through the accessibility of reporter cysteines. *J. Gen. Physiol.* 114:377–392.

Beechem, J.M., and L. Brand. 1985. Time-resolved fluorescence of proteins. *In* Annual Review of Biochemistry. Vol. 54. Annual Reviews, Inc., Palo Alto, CA. 43–71.

Bishop, W.H., L. Henke, J.P. Christopher, and D.B. Millar. 1980. Photodestruction of acetylcholinesterase. *Proc. Natl. Acad. Sci. USA.* 77:1980–1982.

Booth, J.A., A. von Muralt, and R. Stampfli. 1950. The photochemical action of ultraviolet light on isolated single nerve fibers. *Helv. Physiol. Acta.* 8:110–127.

Brown, R.L., S.D. Snow, and T.L. Haley. 1998. Movement of gating machinery during the activation of rod cyclic nucleotide–gated channels. *Biophys. J.* 75:825–833.

Bucossi, G., M. Nizzari, and V. Torre. 1997. Single-channel properties of ionic channels gated by cyclic nucleotides. *Biophys. J.* 72: 1165–1181.

Busath, D.D., and E. Hayon. 1988. Ultraviolet flash photolysis of gramicidin-doped lipid bilayers. *Biochim. Biophys. Acta.* 944:73–78.

Busath, D.D., and R.C. Waldbillig. 1983. Photolysis of gramicidin A channels in lipid bilayers. *Biochim. Biophys. Acta.* 736:28–38.

Callomon, J.H., T.M. Dunn, and I.M. Mills. 1966. Rotational analysis of the 2600 A system of benzene. *Phil. Trans. Roy. Soc. Lond. A Math. Phys. Sci.* 259:499–532.

Calvert, J.G., and J.N. Pitts. 1966. Photochemistry. John Wiley & Sons, Inc., New York, NY. 899 pp.

Chothia, C. 1975. Structural invariants in protein folding. *Nature.* 254:304–308.

Cooper, D.R., and R.J. Davidson. 1965. The effect of ultraviolet light on soluble collagen. *Biochem. J.* 97:139–147.

Creed, D. 1984a. The photophysics and photochemistry of the near-UV absorbing amino acids. I. Tryptophan and its simple derivatives. *Photochem. Photobiol.* 39:537–562.

Creed, D. 1984b. The photophysics and photochemistry of the near-UV absorbing amino acids-II. tyrosine and its simple derivatives. *Photochem. Photobiol.* 39:563–575.

Creed, D. 1984c. The photophysics and photochemistry of the near-UV absorbing amino acids. III. Cystine and its simple derivatives. *Photochem. Photobiol.* 39:577–583.

Creighton, T.E. 1993. Proteins: Structures and Molecular Properties. 2nd ed. W.H. Freeman and Co., New York, NY. 507 pp.

DeFelice, L.J. 1981. Introduction to Membrane Noise. Plenum Publishing Corp., New York, NY. 500 pp.

Dhallan, R.S., K.W. Yau, K.A. Schrader, and R.R. Reed. 1990. Primary structure and functional expression of a cyclic nucleotide-activated channel from olfactory neurons. *Nature.* 347:184–187.

Fesenko, E.E., S.S. Kolesnikov, and A.L. Lyubarsky. 1985. Induction by cyclic GMP of cationic conductance in plasma membrane of retinal rod outer segment. *Nature.* 313:310–313.

Finn, J.T., J. Li, and K.-W. Yau. 1995. C-Terminus involvement in the gating of cyclic nucleotide-activated channels in rod photoreceptors. *Biophys. J.* 68:A253 (Abstr.)

Fodor, A.A., K.D. Black, and W.N. Zagotta. 1997a. Tetracaine reports a conformational change in the pore of cyclic nucleotide-gated channels. *J. Gen. Physiol.* 110:591–600.

Fodor, A.A., S.E. Gordon, and W.N. Zagotta. 1997b. Mechanism of tetracaine block of cyclic nucleotide–gated channels. *J. Gen. Physiol.* 109:3–14.

Fox, J.M., and R. Stampfli. 1971. Modification of ionic membrane currents of Ranvier nodes by UV-radiation under voltage clamp

conditions. *Experientia (Basel)*. 27:1289–1290.

Fujimori, E. 1966. Ultraviolet light irradiated collagen macromolecules. *Biochemistry*. 5:1034–1040.

Goodman, L., and R.P. Rava. 1983. Two-photon spectroscopy of perturbed benzenes. *Adv. Chem. Phys.* 54:177–230.

Gordon, S.E., J.C. Oakley, M.D. Varnum, and W.N. Zagotta. 1996. Altered ligand specificity by protonation in the ligand binding domain of cyclic nucleotide-gated channels. *Biochemistry*. 35: 3994–4001.

Gordon, S.E., M.D. Varnum, and W.N. Zagotta. 1997. Direct interaction between amino- and carboxyl-terminal domains of cyclic nucleotide–gated channels. *Neuron*. 19:431–441.

Gordon, S.E., and W.N. Zagotta. 1995a. A histidine residue associated with the gate of the cyclic nucleotide–activated channels in rod photoreceptors. *Neuron*. 14:177–183.

Gordon, S.E., and W.N. Zagotta. 1995b. Localization of regions affecting an allosteric transition in cyclic nucleotide–activated channels. *Neuron*. 14:857–864.

Goulding, E.H., J. Ngai, R.H. Kramer, S. Colicos, R. Axel, S.A. Siegelbaum, and A. Chess. 1992. Molecular cloning and single-channel properties of the cyclic nucleotide–gated channel from catfish olfactory neurons. *Neuron*. 8:45–58.

Goulding, E.H., G.R. Tibbs, and S.A. Siegelbaum. 1994. Molecular mechanism of cyclic-nucleotide–gated channel activation. *Nature*. 372:369–374.

Grossweiner, L.I. 1976. Photochemical inactivation of enzymes. *Curr. Top. Rad. Res. Q.* 11:141–199.

Haynes, L.W., A.R. Kay, and K.W. Yau. 1986. Single cyclic GMP-activated channel activity in excised patches of rod outer segment membrane. *Nature*. 321:66–70.

Hibbard, L.B., N.J. Kirk, and R.F. Borkman. 1985. The effect of pH on the aerobic and anaerobic photolysis of tryptophan and some tryptophan-containing dipeptides. *Photochem. Photobiol.* 42:99–106.

Hille, B. 1992. Ionic Channels of Excitable Membranes. 2nd ed. Sinauer Associates, Inc., Sunderland, MA. 607 pp.

Hsu, S.-F., G.P. Ahern, and M.B. Jackson. 1999. Ultra-violet light-induced changes in membrane properties in secretory cells. *J. Neurosci. Methods*. 90:67–79.

Jones, D., E. Hayon, and D. Busath. 1986. Tryptophan photolysis is responsible for gramicidin-channel inactivation by ultraviolet light. *Biochim. Biophys. Acta*. 861:62–66.

Kaupp, U.B., T. Niidome, T. Tanabe, S. Terada, W. Bönigk, W. Stühmer, N.J. Cook, K. Kangawa, H. Matsuo, T. Hirose, et al. 1989. Primary structure and functional expression from complementary DNA of the rod photoreceptor cyclic GMP–gated channel. *Nature*. 342:762–766.

Kazutomo, J. 1955. The ultraviolet inactivation of pepsin. *Biochim. Biophys. Acta*. 18:216–220.

Kramer, R.H., and G.R. Tibbs. 1996. Antagonists of cyclic nucleotide–gated channels and molecular mapping of their site of action. *J. Neurosci*. 16:1285–1293.

Kunz, L., U. Zeidler, K. Haegele, M. Przybylski, and G. Stark. 1995. Photodynamic and radiolytic inactivation of ion channels formed by gramicidin A: oxidation and fragmentation. *Biochemistry*. 34:11895–11903.

Lakowicz, J.R. 1983. Principles of Fluorescence Spectroscopy. Plenum Publishing Corp., New York, NY. 496 pp.

Lieberman, E.M. 1970. Ultraviolet radiation effects on isolated nerve fibers. *Adv. Biol. Med. Phys*. 13:329–350.

Liu, D.T., G.R. Tibbs, P. Paoletti, and S.A. Siegelbaum. 1998. Constraining ligand-binding site stoichiometry suggests that a cyclic nucleotide–gated channel is composed of two functional dimers. *Neuron*. 21:235–248.

Liu, D.T., G.R. Tibbs, and S.A. Siegelbaum. 1996. Subunit stoichiometry of cyclic nucleotide–gated channels and effects of subunit order on channel function. *Neuron*. 16:983–990.

Liu, M., T.Y. Chen, B. Ahamed, J. Li, and K.W. Yau. 1994. Calcium-calmodulin modulation of the olfactory cyclic nucleotide–gated cation channel. *Science*. 266:1348–1354.

Ludwig, J., T. Margalit, E. Eismann, D. Lancet, and U.B. Kaupp. 1990. Primary structure of cAMP-gated channel from bovine olfactory epithelium. *FEBS Lett*. 270:24–29.

Luse, R.A., and A.D. McLaren. 1963. Mechanism of enzyme inactivation by ultraviolet light and the photochemistry of amino acids (at 2537 A). *Photochem. Photobiol*. 2:343–360.

Lynch, J.W. 1998. Nitric oxide inhibition of the rat olfactory cyclic nucleotide–gated cation channel. *J. Membr. Biol*. 165:227–234.

Maiti, S., J.B. Shear, R.M. Williams, W.R. Zipfel, and W.W. Webb. 1997. Measuring serotonin distribution in live cells with three-photon excitation. *Science*. 275:530–532.

Matthews, K.S., H.R. Matthews, H.W. Thielmann, and G. Jardetzky. 1973. Ultraviolet difference spectra of the lactose repressor protein. *Biochim. Biophys. Acta*. 295:159–165.

McKim, S., and J.F. Hinton. 1993. Direct observation of differential UV photolytic degradation among the tryptophan residues of gramicidin A in sodium dodecyl sulfate micelles. *Biochim. Biophys. Acta*. 1153:315–321.

McLaren, A.D., and R.A. Luse. 1961. Mechanism of inactivation of enzyme proteins by ultraviolet light. *Science*. 134:836–837.

McLaren, A.D., and S. Pearson. 1949. Effect of pH and urea on ultraviolet light inactivation of crystalline pepsin. *J. Polym. Sci*. 4:45–48.

McLaren, A.D., and D. Shugar. 1964. Photochemistry of Proteins and Nucleic Acids. The MacMillan Co., New York, NY. 449 pp.

Mendez, F., and R. Penner. 1998. Near-visible ultraviolet light induces a novel ubiquitous calcium-permeable cation current in mammalian cell lines. *J. Physiol*. 507:365–377.

Middendorf, T.R., C. Adams, D.A. Baylor, and R.W. Aldrich. 1995. Modification of ion channels by ultraviolet light. *Biophys. J*. 68: A3. (Abstr.)

Middendorf, T.R., and R.W. Aldrich. 2000. Effects of ultraviolet modification on the gating energetics of cyclic nucleotide–gated channels. *J. Gen. Physiol*. 116:253–282.

Miller, S., J. Janin, A.M. Lesk, and C. Chothia. 1987. Interior and surface of monomeric proteins. *J. Mol. Biol*. 196:641–656.

Monod, J., J. Wyman, and J.P. Changeux. 1965. On the nature of allosteric transitions: a plausible model. *J. Mol. Biol*. 12:88–118.

Morrill, J.A., and R. MacKinnon. 1999. Isolation of a single carboxyl–carboxylate proton binding site in the pore of a cyclic nucleotide-gated channel. *J. Gen. Physiol*. 114:71–83.

Nakamura, T., and G.H. Gold. 1987. A cyclic nucleotide–gated conductance in olfactory receptor cilia. *Nature*. 325:442–444.

Noren, C.J., S.J. Anthony-Cahill, M.C. Griffith, and P.G. Schultz. 1989. A general method for site-specific incorporation of unnatural amino acids into proteins. *Science*. 244:182–188.

Nowak, M.W., J.P. Gallivan, S.K. Silverman, C.G. Labarca, D.A. Dougherty, and H.A. Lester. 1998. In vivo incorporation of unnatural amino acids into ion channels in *Xenopus* oocyte expression system. *Methods Enzymol*. 293:504–529.

Nozaki, Y., and C. Tanford. 1971. The solubility of amino acids and two glycine peptides in aqueous ethanol and dioxane solutions. Establishment of a hydrophobicity scale. *J. Biol. Chem*. 246:2211–2217.

Oxford, G.S., and J.P. Pooler. 1975. Ultraviolet photoalteration of ion channels in voltage-clamped lobster giant axons. *J. Membr. Biol*. 20:13–30.

Paoletti, P., E.C. Young, and S.A. Siegelbaum. 1999. C-Linker of cyclic nucleotide–gated channels controls coupling of ligand binding to channel gating. *J. Gen. Physiol*. 113:17–34.

Peters, R., J. Peters, K.H. Tews, and W. Bahr. 1974. Microfluorimetric study of translational diffusion of proteins in erythrocyte membrane. *Biochim. Biophys. Acta.* 367:282–294.

Radzicka, A., and R. Wolfenden. 1988. Comparing the polarities of the amino acids: side-chain distribution coefficients between the vapor phase, cyclohexane, 1-octanol, and neutral aqueous solution. *Biochemistry.* 27:1664–1670.

Richards, F.M. 1974. The interpretation of protein structures: total volume, group volume distributions, and packing density. *J. Mol. Biol.* 82:1–14.

Saks, M.E., J.R. Sampson, M.W. Nowak, P.C. Kearney, F. Du, J.N. Abelson, H.A. Lester, and D.A. Dougherty. 1996. An engineered Tetrahymena tRNAGln for in vivo incorporation of unnatural amino acids into proteins by nonsense suppression. *J. Biol. Chem.* 271:23169–23175.

Setlow, J.K. 1961. Ultraviolet inactivation of transforming DNA. *Radiat. Res.* 14:500. (Abstr.)

Setlow, R., and B. Doyle. 1954. The effect of temperature on the ultraviolet light inactivation of trypsin. *Arch. Biochem. Biophys.* 48: 441–447.

Setlow, R., and B. Doyle. 1957. The action of monochromatic ultraviolet light on proteins. *Biochim. Biophys. Acta.* 24:27–41.

Steinfeld, J.I. 1985. Molecules and Radiation. 2nd ed. The MIT Press, Cambridge, MA. 493 pp.

Strassle, M., G. Stark, M. Wilhelm, P. Daumas, F. Heitz, and R. Lazaro. 1989. Radiolysis and photolysis of ion channels formed by analogues of gramicidin A with a varying number of tryptophan residues. *Biochim. Biophys. Acta.* 980:305–314.

Stühmer, W., and W. Almers. 1982. Photobleaching through glass micropipettes: sodium channels without lateral mobility in the sarcolemma of frog skeletal muscle. *Proc. Natl. Acad. Sci. USA.* 79: 946–950.

Sun, Z.P., M.H. Akabas, E.H. Goulding, A. Karlin, and S.A. Siegelbaum. 1996. Exposure of residues in the cyclic nucleotide–gated channel pore: *P* region structure and function in gating. *Neuron.* 16:141–149.

Tallmadge, D.H., and R.F. Borkman. 1990. The rates of photolysis of the four individual tryptophan residues in UV exposed calf gamma-II crystallin. *Photochem. Photobiol.* 51:363–368.

Tibbs, G.R., E.H. Goulding, and S.A. Siegelbaum. 1997. Allosteric activation and tuning of ligand efficacy in cyclic-nucleotide–gated channels. *Nature.* 386:612–615.

Turro, N.J. 1978. Modern Molecular Photochemistry. Benjamin/Cummings Publishing Co., Inc., Menlo Park, CA. 628 pp.

Varnum, M.D., K.D. Black, and W.N. Zagotta. 1995. Molecular mechanism for ligand discrimination of cyclic nucleotide–gated channels. *Neuron.* 15:619–625.

Varnum, M.D., and W.N. Zagotta. 1997. Interdomain interactions underlying activation of cyclic nucleotide–gated channels. *Science.* 278:110–113.

Vladimirov, Y.A., D.I. Roshchupkin, and E.E. Fesenko. 1970. Photochemical reactions in amino acid residues and inactivation of enzymes during U.V.-irradiation. A review. *Photochem. Photobiol.* 11: 227–246.

Walrant, P., and R. Santus. 1974. *N*-Formyl-kynurenine, a tryptophan photooxidation product, as a photodynamic sensitizer. *Photochem. Photobiol.* 19:411–417.

Wang, L., D. Xu, W. Dai, and L. Lu. 1999. An ultraviolet-activated K^+ channel mediates apoptosis of myeloblastic leukemia cells. *J. Biol. Chem.* 274:3678–3685.

Weber, G. 1960. Fluorescence-polarization spectrum and electronic-energy transfer in tyrosine, tryptophan, and related compounds. *Biochem. J.* 75:335–345.

Yariv, A. 1975. Quantum Electronics. 2nd ed. John Wiley & Sons, Inc., New York, NY. 570 pp.

Yau, K.W., and D.A. Baylor. 1989. Cyclic GMP–activated conductance of retinal photoreceptor cells. *Annu. Rev. Neurosci.* 12:289–327.

Zimmerman, A.L., and D.A. Baylor. 1986. Cyclic GMP–sensitive conductance of retinal rods consists of aqueous pores. *Nature.* 321:70–72.

Zimmerman, A.L., J.W. Karpen, and D.A. Baylor. 1988. Hindered diffusion in excised membrane patches from retinal rod outer segments. *Biophys. J.* 54:351–355.

Zong, X., H. Zucker, F. Hofmann, and M. Biel. 1998. Three amino acids in the C-linker are major determinants of gating in cyclic nucleotide–gated channels. *EMBO (Eur. Mol. Biol. Organ.) J.* 17: 353–362.